Peridynamics modeling of hydraulic fracture interaction with natural fractures in fractured rock mass

Mingqi Qin, Diansen Yang, Yun Jia, Yun Zhou

Journal Pre-proofs

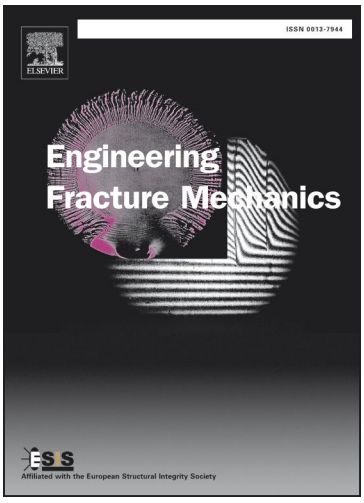

Peridynamics modeling of hydraulic fracture interaction with natural fractures in fractured rock mass

MingqiQin, Diansen Yang, Yun Jia, Yun Zhou

PII: S0013-7944(24)00462-4
DOI: https://doi.org/10.1016/j.engfracmech.2024.110299
Reference: EFM 110299

To appear in: *Engineering Fracture Mechanics*

Received Date: 21 March 2024
Revised Date: 15 May 2024
Accepted Date: 9 July 2024

Please cite this article as: MingqiQin, Yang, D., Jia, Y., Zhou, Y., Peridynamics modeling of hydraulic fracture interaction with natural fractures in fractured rock mass, *Engineering Fracture Mechanics* (2024), doi: https://doi.org/10.1016/j.engfracmech.2024.110299

Peridynamics Modeling of Hydraulic Fracture Interaction with Natural Fractures in Fractured Rock Mass

MingqiQin[a], Diansen Yang[a*], Yun Jia[b], Yun Zhou[c]

[a]School of Civil Engineering, Wuhan University, Wuhan 430072, Hubei, China

[b]Universit´e de Lille, CNRS, Centrale Lille, UMR 9013 - LaMcube - Laboratoire de M´ecanique, Multiphysique, Multi-´echelle, F-59000 Lille, France

[c]Institute of Rock and Soil Mechanics, Chinese Academy of Sciences, Wuhan, Hubei 430071, China

Abstract

In this paper, hydraulic fracturing in fractured rock masses are studied using peridynamics, with a special attention to the interaction mechanisms between hydraulic fractures (HFs) and natural fractures (NFs). To achieve this objective, a two-dimensional numerical model is firstly analyzed to understand the effects of the in-situ stress, fracturing fluid viscosity, fracturing fluid injection rate, fracture friction coefficient and fracture approach angle on the interaction between HFs and NFs. The obtained results reveal that larger in-situ stress ratio, elevated friction coefficient, increased fluid viscosity, enhanced injection rate and wider approach angle create more favorable conditions for HF penetration into NF. After that, the fracture morphologies in fractured rock are analyzed under three-dimensional, successfully reproducing the 'diversion' interaction pattern between fractures, a phenomenon unattainable in 2D modeling. It was observed that there exists a mixed interaction mode between penetration and diversion, particularly when the length of NF is limited and the angle between NF and HF is less than 90°. Finally, the propagation of HFs within a 3D fractured rock mass featuring arbitrarily distributed joints (NFs) is simulated, providing new insights into complex real-world scenarios.

Key words: Hydraulic fracturing; Peridynamics; Jointed rock; Interaction mechanism; Three-dimensional modeling.

1. Introduction

Hydraulic fracturing in fractured rock formations is a challenging task. In fracturing operations, the discontinuous interfaces, natural fractures (NFs) and joints will interact with hydraulic fractures (HFs), affecting the propagation of HFs. The existence of NFs and joints will also have an important impact on the formation of HF

*Corresponding author.
E-mail address: dsyang@whu.edu.cn(D. Yang)

networks. The study of the interaction mechanisms between HFs and NFs is crucial for the construction and design of hydraulic fracturing in fractured reservoirs.

In practice, understanding the interaction mechanisms between HF and NF presents an important challenge due to the absence effective criteria for predicting the interaction patterns and outcomes among the fractures. The theory of linear elastic fracture mechanics (LEFM) is generally used to judge crack propagation based on geometric information, such as position and direction at the crack tip. However, when a HF is close to a NF, and the HF tip may coincide with the NF, the specific geometric information of the fracture tip cannot be obtained, and the propagation direction of the HF cannot be judged by the LEFM theory. Therefore, the interaction mechanism between HFs and NFs can hardly be analyzed and simulated by LEFM theory.

Some scholars have studied the interaction mechanism between HFs and NFs by analyzing field data or experimental data. Warpinski and Teufel[1] conducted a theoretical analysis based on the measured data of a mining site and considered that the in-situ stress difference is the main factor determining whether HF can penetrate NF. Blanton[2, 3] analyzed experimentally the influence of the approach angle and principal stress difference on the interaction between HF and NF experimentally. The closer the approach angle was to 90°, the easier HF passed through NF. Bunger et al.[4] further studied the effect of approach angle on propagation morphology when a HF penetrated a NF. Based on the experimental results, Beugelsdijk et al.[5] summarized the effect of the stress distribution on the crack shape during the interaction of a HF and NF. Llanos et al.[6] studied the influence of different factors such as the friction coefficient of NF surface and viscosity of the fracturing fluid on the interaction between HFs and NFs and pointed out that the higher the friction coefficient and viscosity of the fracturing fluid, the more conducive it was to the HF penetrating the NF. Guo et al.[7] also studied the influence of in-situ stress distribution, fracturing fluid viscosity and treatment volume on the HF propagation in fractured rock masses based on true triaxial tests. They pointed out that reasonable fracturing fluid viscosity and displacement were the key factors, controlling the fracturing effect in the studied fractured rock masses. In addition, Hanson et al.[8, 9], Pippan et al.[10], and other scholars[1, 11] compared the effects of the in-situ stress distribution, friction coefficient, approach angle and other factors on the interaction processes between HFs and NFs. These obtained experimental studies revealed that the influence of various factors on the interaction between HFs and NFs. However, it is still difficult to analyze the interaction mechanism between HF and NF because these tests cannot directly obtain crucial physical quantities, such as stress distribution, pressure distribution and fracture aperture.

To explain the observed phenomena and quantitatively analyze the interaction between HFs and NFs, series of theoretical analysis have been performed. Blanton et al.[2] proposed a criterion to judge whether a HF can pass through a NF. In the experimental tests, HF and NF were assumed to be perpendicular to each other with

the neglect of the influence of fracturing fluid flow. According to this criterion, the rock mass located on the side of the NF that is away from the HF may experience tension-induced damage. Warpinski and Teufel[12] assumed that when the fracturing fluid pressure at the intersection was higher than the normal stress on the NF surface, the NF opened, On the other hand, when the rock mass slipped on both sides of the NF, the HF could not penetrate the NF and consequently proposed a penetration criterion considering the fracturing fluid pressure. Renshaw and Pollard[13] proposed a criterion (the RP criterion) to verify whether a HF can penetrate a NF when the approach angle is 90°. Gu and Wen[14] and Sarmadivaleh[15] improved the criterion to judge whether HFs could penetrate NFs at any approach angle. In addition, Anderson[16], Hanson et al.[17] and other scholars[18-20] theoretically analyzed the influence of the friction coefficient, in-situ stress ratio and approach angle on the interaction between HFs and NFs. These theoretical models often require additional assumptions for simplification, and the models suitable for these criteria need to satisfy certain geometric and boundary conditions (for example, the HF and the NF should be perpendicular to each other), so they are difficult to apply to numerical simulation and engineering design.

In parallel, a number of researchers have investigated the interaction mechanism between HFs and NFs by numerical simulation. Shi et al.[21], Kohei et al.[22] and Wang et al.[23] simulated the propagation process of a HF approaching a NF using the extended finite element method (XFEM). However, due to the limitation of LEFM theory, these models cannot judge the propagation path after the convergence of HF and NF. After that, based on the previous theoretical research results mentioned above, some scholars have improved the XFEM model to judge the propagation path of cracks after HFs interact with NFs[24-26]. In addition, some scholars have simulated the interaction process between HFs and NFs based on the displacement discontinuous method (DDM) and finite element method (FEM) and studied the influence mechanism of in-situ stress, layer properties, friction coefficient and approach angle on the interaction process between fractures[27-34]. Zhang et al.[35] have numerically investigated the process of HFs intersecting with NFs, and pointed out that the factures' offsets can hinder hydraulic opening of segments under high compression, reducing their permeability and consequently increasing overall upstream fracture pressure and opening. Moreover, they observed that some injected fluid is lost into closed empty fractures intersecting the main HF, thereby delaying the necessary pressure increases for growth beyond the intersecting fracture. Behnia et al.[36] studied the influence of the relative positions (approach angle and distance) between HFs and NFs on the propagation path of HF based on DDM. Moradi et al.[37] used the higher-order displacement discontinuous method (HODDM) to simulate the propagation of HF in rock masses containing NFs. They proposed a criterion to assess the interaction between HF and NF, noting the potential for HF to penetrate opened NFs. Additionally they observed that once HF penetrates an NF, subsequent penetrations decrease due to the decrease in fracturing fluid pressure. Zhang et al.[38] simulated hydraulic fracturing in rock masses containing complex NF networks using DDM. They pointed out that the most complex fracture patterns can

be obtained when the maximum principal stress direction is perpendicular to the principle natural fracture direction. Moreover, they found that increasing viscosity can mitigate the adverse effects of stress anisotropy on fracturing efficiency. These methods based on LEFM theory and traditional continuum mechanics still have some problems in judging the initiation of newly generated cracks after HFs interact with NFs. To overcome these problems, some scholars have used the discrete element method (DEM)[39-43], the virtual multidimensional internal bond (VMIB) method[44]and the FEM with damage elements[45, 46]. Compared with traditional methods such as XFEM and BEM, these methods have advantages to simulate the interaction process between HFs and NFs without additional assumptions. To numerically study hydraulic fracturing in fractured rock masses more effectively, it is necessary to solve the problem of fracture initiation (accompanied by penetration, capture, offset, etc.) when the HFs interacts with the NFs and obtain sufficient physical information (fracturing fluid pressure, fracture aperture, stress distribution) to analyze the mechanism of interaction between the HFs and the NFs. Therefore, it is necessary to establish a numerical framework that can not only simulate the interaction between fractures without additional assumptions and criteria but also obtain detailed physical information.

Peridynamics (PD)[47-49] is a recently developed numerical analysis method based on nonlocal theory. PD solves physical fields by calculating integral in the neighborhood of particles instead using differential calculations. It no longer distinguishes between continuity and discontinuity, making it highly suitable for modeling systems with arbitrarily distributed non-continuous interfaces. Based on these characteristics, this paper establishes the hydraulic fracturing model based on PD. Because the PD-based numerical framework is not constrained by the LEFM theory, our model can simulate the interaction between HFs and NFs in a fractured rock mass more effectively.

This paper employs a two-dimensional hydraulic fracturing numerical model to comprehensively investigate the interaction mechanisms between HF and NF. The study also explores the specific influences of geological conditions (in-situ stress distribution), rock mechanics properties (friction coefficient), and construction parameters (fracturing fluid viscosity and injection rate) on the interaction process. Afterwards, utilizing a fully three-dimensional hydraulic fracturing numerical model, the interaction patterns between HF and NF in three-dimensional rock mass will be investigated. This revealed interaction modes between fractures that cannot be studied through two-dimensional models. Finally, a fully three-dimensional fractured rock mass model is constructed to simulate hydraulic fracturing within a rock mass containing arbitrarily distributed natural fractures. The study focused on the propagation patterns and distribution laws of HFs within the fractured rock mass.

2. Hydraulic fracturing model of a fractured rock mass based on PD

Based on the advantages of PD in simulating rock-like material fracture and

progressive failure, we have developed and tested a 2D/3D fluid structure coupling PD-based numerical framework for hydraulic fracturing[50, 51]. On the basis of our self-developed hydraulic fracturing numerical model, this paper combines the previously proposed PD contact-friction model, PD interface model[52], bond-breaking criterion based on bond stress[53], and parallel computing based calculation method[50] to establish a fractured rock mass numerical model, and applies it to the investigation of hydraulic fracturing and the interaction mechanism between fractures.

2.1. PD-based model of the fractured rock

In the PD-based model, a material point interacts with other material points within its influence domain (referred to as the "family" region) through "bonds". The interaction force between material points is termed as “bond force”. The equation of motion for a material point can be written as[54]

$$\rho(x)\ddot{\mathbf{u}}(x,t) = \int_{H_x} \mathbf{F}(\boldsymbol{\xi},t)\mathrm{d}V_{x'} + \mathbf{F_b}(x,t) + \int_{H_x} \mathbf{T}(\boldsymbol{\xi},t)\mathrm{d}V_{x'} \tag{1}$$

where H_x is the influence domain of the material. $\boldsymbol{\xi}$ is the relative position vector between the material points ($\boldsymbol{\xi}=\mathbf{x}'-\mathbf{x}$). $V_{x'}$ is the volume of the material point. $\mathbf{F_b}(x,t)$ is the body force density of the material point x. $\mathbf{F}(\boldsymbol{\xi},t)$ is the bond force density between the material points associated with the elongation, which can be express as

$$\mathbf{F}(\boldsymbol{\xi},t) = C\frac{|\boldsymbol{\xi}+\boldsymbol{\eta}|-|\boldsymbol{\xi}|}{|\boldsymbol{\xi}|}\mu(\boldsymbol{\eta},\boldsymbol{\xi},t)\cdot\frac{\boldsymbol{\xi}+\boldsymbol{\eta}}{|\boldsymbol{\xi}+\boldsymbol{\eta}|}dV_{x'} \tag{2}$$

where C is the micro modulus[49], $\boldsymbol{\eta}$ is the relative displacement vector of the material points on the either side of the bond($\boldsymbol{\eta}=\mathbf{u}_{x'}-\mathbf{u}_x$). $\mu(\boldsymbol{\eta},\boldsymbol{\xi},t)$ is a historical scalar indicating whether the bond is broken. When the bond between two material points is broken, the value is 0; otherwise, the value is 1.

$\mathbf{T}(\boldsymbol{\xi},t)$ in Equation (1) represents the equivalent repulsive force applied to the pairs of material points on either side of the broken bond, used to simulate the effect of fluid pressure. Its expression is[55]:

$$\left|\mathrm{T}(\boldsymbol{\xi},t)\right| = \begin{cases} \dfrac{6P}{\pi\delta^3} & \text{for 2D} \\ \dfrac{6P}{\pi\delta^4} & \text{for 3D} \end{cases} \tag{3}$$

As mentioned in the first chapter, frictional forces play a significant role in the interaction between HFs and NFs. Investigating the influence mechanism of frictional on the interaction between the HF and the NF is one of the main focuses of this paper.

The contact-friction model we developed earlier for PD-based models is capable of effectively simulating hydraulic fracturing in a jointed rock mass[55, 56].

In the contact-friction model applicable to PD, there may be normal contact force and frictional force between the adjacent particles if the bond between them has been broken ($|\boldsymbol{\xi}| = \Delta x$,$\mu(\boldsymbol{\eta},\boldsymbol{\xi},t)=0, |\boldsymbol{\xi}+\boldsymbol{\eta}| \le \Delta x$). The normal contact force is expressed as[55, 56]

$$\mathbf{F}_{\mathbf{con}}(\boldsymbol{\xi},t) = \min\left(\alpha\frac{C}{\delta}S_n, 0\right)\mathbf{n}\cdot dV_{x'} \tag{4}$$

where S_n is the relative normal displacement between the adjacent material points, $\mathbf{n}$ is the unit normal vector, and α is the adjustment coefficient (in this paper, α=2).

According to Coulomb's law of friction, during the static friction phase ($|\mathbf{F}_{\mathbf{fri}}| \le \mu_{fri}|\mathbf{F}_{\mathbf{con}}|$), the static friction between the adjacent points can be written as

$$\mathbf{F}_{\mathbf{fri0}}(\boldsymbol{\xi},t) = \beta\frac{C}{\delta}S_{\mathrm{t}}'\mathbf{t}\cdot dV_{x'} \tag{5}$$

$$S'_t = S_t - S^0_{slide} \tag{6}$$

where $\mathbf{t}$ is the unit tangential vector of the relative displacement, β is the adjustment coefficient (in this paper, α=3). S_t' is the increment of relative tangential displacement, S_t is the relative displacement and S^0_{slide} is the historical relative sliding displacement. When the direction of the relative tangential velocity between the points is opposite to the direction of the relative tangential displacement, the value of S^0_{slide} is updated to S_t.

In addition to the contact-friction model applicable to PD, we have also proposed a cohesive interface model suitable for PD (please refer to the published literature[57, 58]), which is crucial for simulating hydraulic fracturing of fractured rock masses.

In PD, material damage is characterized by the breakage of bonds between material points. When a bond breaks, there is no longer interaction between the material points on either side of that bond[47]. In the classical PD-based model, when the elongation rate of a bond exceeds a critical elongation rate S_0 that is related to the material's fracture energy G_c, bulk modulus k, and the radius of the material point's family δ (as shown in Equation (7)), the bond will fracture ($\mu(\boldsymbol{\eta},\boldsymbol{\xi},t)=0$)[59].

$$S_0 = \begin{cases} \sqrt{\dfrac{\pi G_c}{3k\delta}} & \text{for 2D} \\ \sqrt{\dfrac{5\pi G_c}{9k\delta}} & \text{for 3D} \end{cases} \tag{7}$$

The aforementioned bond-breaking criterion based on critical elongation rate is inadequate for predicting shear failure, which plays a significant role in underground engineering. Therefore, in our previous research, we have developed a bond-breaking criterion based on the bond stress (Please refer to the published literature for details[50]).

The damage value of a material point is calculated using the following equation:

$$D(\mathbf{x},t)=1-\frac{\int_{H_x}\mu(\boldsymbol{\eta},\boldsymbol{\xi},t)dV_{\mathbf{x}'}}{\int_{H_x}dV_{\mathbf{x}'}} \tag{8}$$

Equation (9) is employed to determine the locations of macroscopic fracture segments: when the bond between the adjacent material points break, and the damage values of both material points are no less than 0.24, it is considered that there is a macroscopic fracture segment between the adjacent material points. More details on the method for determining the position of macroscopic fractures can be found in our published article[50].

$$\begin{cases} |\boldsymbol{\xi}|=dx \\ \mu(\boldsymbol{\eta},\boldsymbol{\xi},t)=0 \\ D(\mathbf{x},t)\geq 0.24 \\ D(\mathbf{x}',t)\geq 0.24 \end{cases} \tag{9}$$

Due to the absence of intense dynamic responses or dynamic failure in the hydraulic fracturing process, and also to enhance the stability of the numerical model, the calculation of solid displacement adopts the adaptive dynamic relaxation method (ADR)[54, 60].

2.2. Fracturing flow

This paper assumes that the fracturing fluid inside the fractures behaves as steady state laminar flow. The fracture position is determined by Equation (9), and the aperture of the fracture w can be obtained by calculating the relative displacement of material points on either side of the fracture[53]. The flow rate Q per unit volume of material point can be expressed as

$$Q=\rho_f\frac{k_f}{\mu_f}\nabla P \tag{10}$$

where ρ_f is the density of the fracturing fluid, μ_f is the viscosity of the fracturing fluid, and k_f is the permeability of the fracture following the Cubic law as

$$k_f = \frac{w^2}{12} \tag{11}$$

Based on Equations (10), the flow equation in the fracture can be written as

$$Q(\mathrm{x},t) = \sum_{i=1}^{n} q(\xi,t) \cdot A_{x'\mathrm{x}} + I(x,t) \tag{12}$$

$$q(\xi,t) = \gamma \frac{\rho_f}{\mu_f} \frac{k_f}{|\xi|} (P(\mathbf{x}',t) - P(\mathbf{x},t)) \tag{13}$$

where n is the number of fractures connected to fracture segment, $I(x, t)$ is the input flow rate per unit volume of fracture and γ is the volume of the fracture. For a 3D model, when the radius of the family of the fracture δ_f=Δx, $\gamma = \frac{1}{\mathrm{d}x^2 \cdot w}$. q (x, t, ξ) is the flow rate to the fracture segment x along the bond ξ, $A_{xx'}$ is the sectional area of the fracture.

Based on the compressibility of the fluid, the rate of change of hydraulic pressure within the fracture segment can be expressed as

$$\dot{P}(x,t) = \left(\frac{Q(x,t)}{\rho_f} - \frac{\dot{w}(x,t)}{w(x,t_0)} \right) K_f \tag{14}$$

where K_f is the bulk modulus of the fracturing fluid.

Equations (12), (13), and (14) implement simulations of hydraulic fracturing fluid flow within the fractures. Equation (3), along with the terms related to fracture aperture w in Equations (11) and (14), demonstrate that the numerical framework can achieve hydro-mechanical coupling. To ensure the convergence of the model, different time step lengths are selected for the iteration of rock movement and hydraulic pressure during fracturing. Specifically, the time step length Δt_f chosen for simulating hydraulic fluid flow is significantly shorter than the time step length Δt_s selected for simulating rock movement. To maximize computational efficiency while ensuring model convergence, within each main time step Δt, the calculation proceeds as follows: first, after computing the flow of fracturing fluid for n time steps, the results (pressure changes) from the fluid flow simulation are incorporated into the calculation of rock displacement. Upon completing the calculation of rock displacement, the results (fracture opening rates) are then utilized for the subsequent n time steps of fracturing fluid flow calculation. It is necessary to satisfy the condition $\Delta t_s = n\Delta t_f = \Delta t$. Due to the significant computational time required for 3D models, parallel computing is introduced in this study to improve the computational efficiency (the parallel computing process is described in our previously published work[56]). The algorithmic flow of the numerical model is illustrated in Fig. 1.

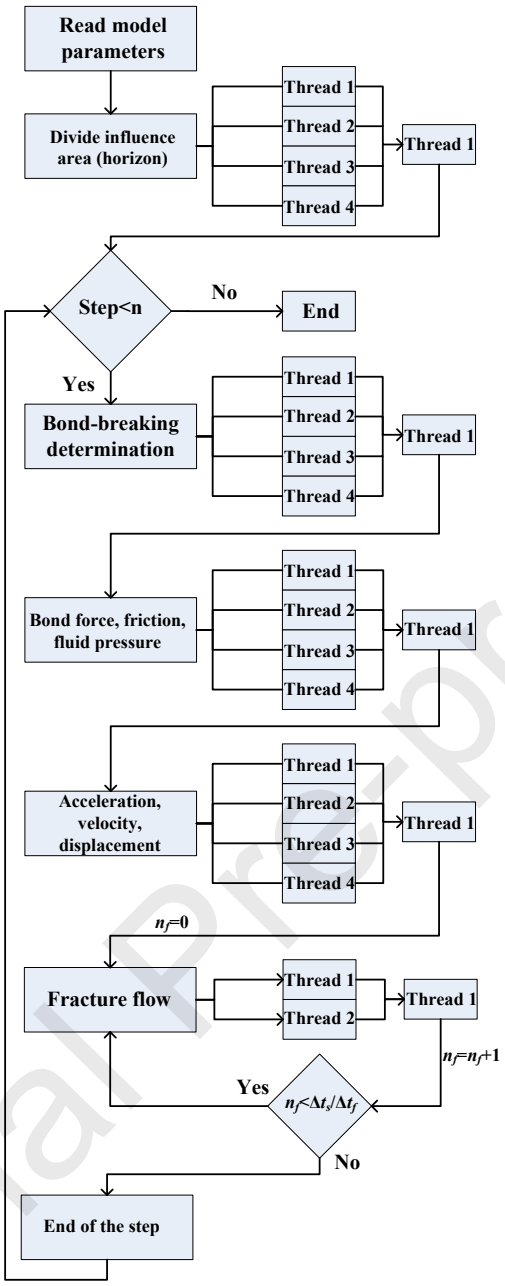

278

279 **Fig. 1.** Algorithm flow chart.

280 The accuracy and performance of the numerical framework used in this paper
281 have been validated in our published works[50, 61].

282 *2.3. Validation of the numerical model for hydraulic fracturing in fractured rock*

283 In our previous work, we have compared the numerical solution of this model with
284 the analytical solution based on the Khristianovich-Geertsma-de Klerk (KGD) model
285 to verify the accuracy of the proposed model[62]. In this paper, the interaction
286 between HFs and NFs is simulated, and the numerical results are compared with the
287 experimental results of Khoei et al.[24]. The numerical model is shown in Fig. 2.
288 There is a single NF in the model, and the displacement around the model is

289 constrained. The test conditions and model parameters are shown in Table 1.

290 **Table 1** Test conditions and model parameters

Specimen	W	H	(x1,y1)	(x2,y2)	y0	Young's modulus E	Poisson's ratio ν
1	111mm	45mm	(30.5,4) (mm, mm)	(55.4.,42.16) (mm, mm)	27.9mm	36.5GPa	0.25
2	110mm	54mm	(55.4,42.16) (mm, mm)	(98.12,46.07) (mm, mm)	26.9mm	32.5GPa	0.25

291

Specimen	Fracture energy G_c	Internal friction angle φ	Cohesive force C
1	330J/m^2	48°	20 MPa
2	330J/m^2	48°	20 MPa

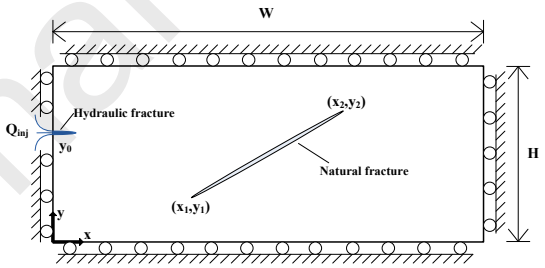

292

293 **Fig. 2.** Numerical model of the studied experimental tests.

294 It can be seen from Figs. 3 and 4 that the numerical simulation of HF
295 propagation path is basically consistent with the experimental results, indicates that
296 the developed model used in this paper is capable of reproducing the interaction
297 process of HFs and NFs correctly.

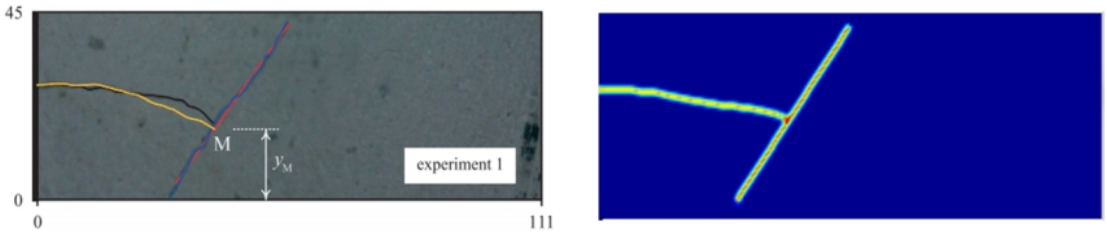

(a) (b)

298 **Fig. 3.** Comparison of test 1 results: (a) experimental results; (b) simulation results.

299

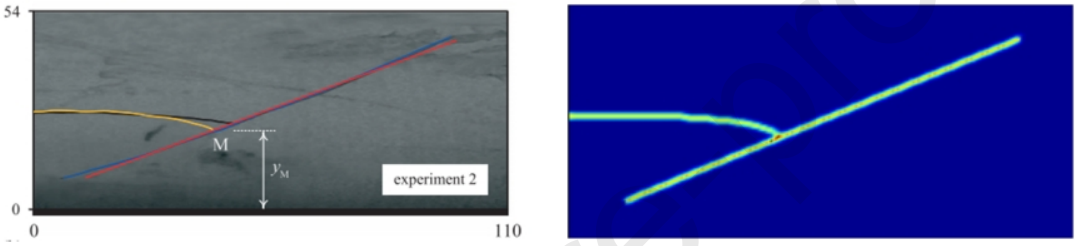

(a) (b)

300 **Fig. 4**. Comparison of test 2results: (a) experimental results; (b) simulation results.

301 **3. Interaction mechanism between HF and NF**

302 When a NF is close to a HF, two competing processes occur simultaneously. One
303 process is that with the opening of HF, the rock mass on the other side of NF will
304 crack under the action of friction (as shown in Fig. 5 (a)). The other one is that the
305 fracturing fluid enters NF and induces the opening of NF, weakening the friction
306 effects on the other side of the NF and preventing it from cracking (as shown in Fig. 5
307 (b)). These two processes compete with each other and influence each other. When
308 the first process is dominated, HF tends to penetrate NF. However, when the second
309 process dominates, HF tends to be captured by NF.

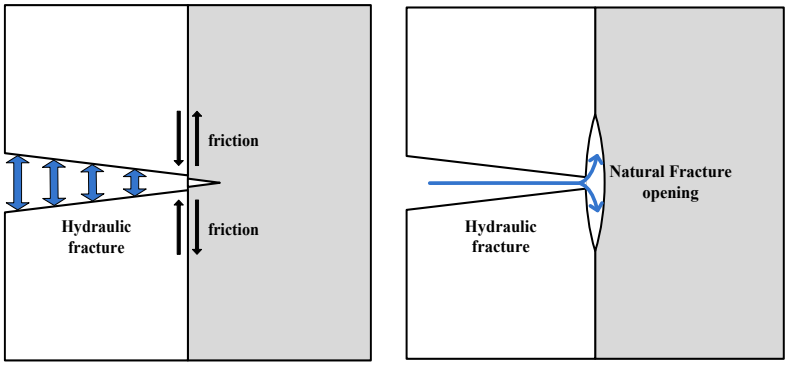

(a) (b)

Fig. 5. Two main processes occur when a NF approaches a HF: (a) the rock mass on the other side of the NF cracks under the friction; (b) the fracturing fluid enters the NF and induces the NF opening.

To study the influence of the friction coefficient, fracturing fluid viscosity, in-situ stress and fracturing fluid injection rate on the interaction results of HF and NF (i.e., the influence of different factors on the above two processes), the 2D model is shown in Fig. 6. The model dimension is 3m * 3m, with an elastic modulus E of the model is 15 GPa, and a Poisson's ratio v of 0.25. The characteristic length Δx of material particles is 0.025 m, and the individual time step Δt is 5e-5 s (where the time step for simulating rock deformation Δt_s is 5e-5 s, and the time step for simulating hydraulic fracturing fluid flow Δt_f is 5e-10 s). There is a vertical NF (noncohesive fracture) in the center of the model. The HF propagates from the left side of the model to the NF. The aperture of NF, the distribution of tensile stress on the right side of the NF and the change in fracturing fluid pressure in NF are observed. This paper will study the mechanisms of interaction between HF and NF by investigating the distribution of in-situ stress (by adjusting the maximum horizontal stress σ_H and minimum horizontal stress σ_h), mechanical properties of fracture surfaces (by adjusting the friction coefficient μ_{fir}), and construction parameters (by adjusting the fracturing fluid viscosity μ_f and injection rate Q). The loading condition and model parameters are given in Table 2.

Table 2 Loading conditions and model parameters of the sample with a vertical NF

Case	Minimum horizontal stress σ_h	Maximum horizontal stress σ_H	Friction coefficient μ_{fir}	Fracturing fluid viscosity μ_f	Injection rate Q
A	3 MPa	4 MPa	0 to 0.65	1e-3 Pa·s	1e-3 m^3/s

B	3 MPa	3 to 6 MPa	0.25	1e-3 Pa·s	1e-3 m^3/s
C	3 MPa	4 MPa	0.25	2.5e-4 to 5e-3 Pa·s	1e-3 m^3/s
D	3 MPa	4MPa	0.25	1e-3 Pa·s	2.5e-4 to 1e-3 m^3/s

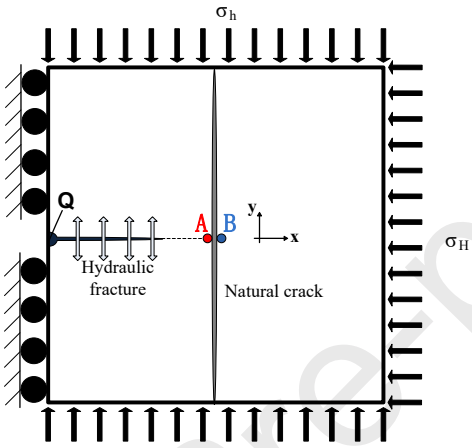

Fig. 6. Diagram of the numerical model with a vertical NF

3.1. Effect of friction coefficient

Case A in Table 2 illustrates the effect of the friction coefficient on the interaction between HF and NF. When HF is close to NF, the change of tensile stress at point B with the change of friction coefficient μ_{fri} is shown in Fig. 7(a). When HF extends to point A (here, 1000 steps after the HF reaches point A is considered), the distribution of tensile stress on the right side of the surface of NF is shown in Fig. 7(b).

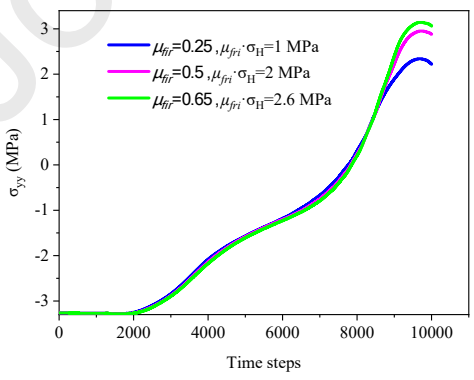

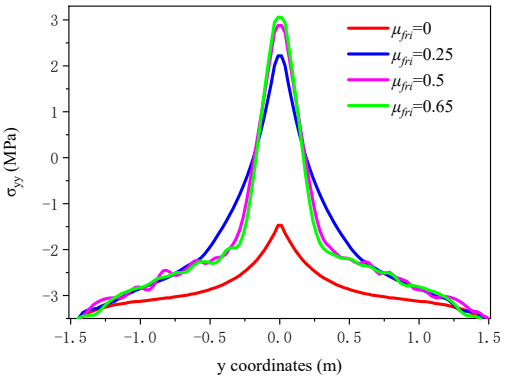

(a) (b)

Fig. 7. Effect of the friction coefficient on the distribution of tensile stress on the right side of the HF: (a) variation curve of tensile stress at point B; (b) distribution of tensile stress on the right side of NF.

The obtained results show that, the tensile stress on the right side of NF increases with friction coefficient, which may induce the HF penetrating the NF. Additionally, Fig. 8(a) indicates that the tensile stress σ_{yy} on the right side of the NF is not directly linearly proportional to the friction coefficient μ_{fri}, while the friction force is significantly higher than $\mu_{fri} \cdot \sigma_H$. This observation is related to the fact that the sliding friction is a typical nonlinear process and then the magnitude of frictional forces acting on the fracture surfaces in each set of cases is not linearly proportional to the friction coefficient. Since the areas of stress concentration near the HF tip (as shown in Fig. 8), the friction force on the right side of NF will be significantly higher than that of $\mu_{fri} \cdot \sigma_H$.

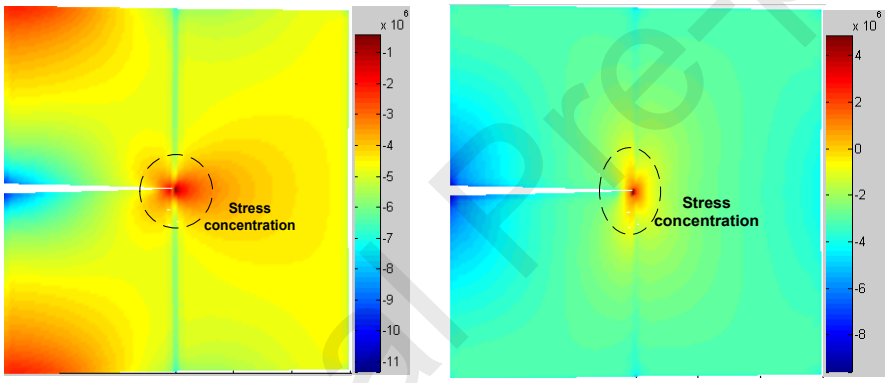

(a) (b)

Fig. 8. Schematic diagram of the stress concentration at the tip of the HF: (a) distribution of σ_{xx}; (b) distribution of σ_{yy}.

3.2. Effect of in-situ stress distribution

Case B illustrates the effect of the in-situ stress distribution (in-situ stress ratio) on the interaction between HF and NF. In hydraulic fracturing, in-situ stress is an important factor affecting the fracturing behavior. When HF is close to NF, the distribution of in-situ stress will affect the contact force of NF surface, thus affecting the friction force on the right side of the NF. At the same time, the distribution of in-situ stress also affects the opening process of NF, as well as the interaction between the HF and the NF. When HF is close to NF, the change in tensile stress at point B is shown in Fig.9(a). When HF extends to point A, the tensile stress distribution on the right side of the NF is shown in Fig. 9(b). The simulation results in Fig. 9 show that with the

increase of in-situ stress ratio, the tensile stress on the right side of the NF increases. Therefore, the greater the in-situ stress ratio is, the more likely the HF is to penetrate the NF. Meanwhile, Fig. 9(a) shows that the in-situ stress ratio has little effect on the crack propagation rate and rock mass deformation rate.

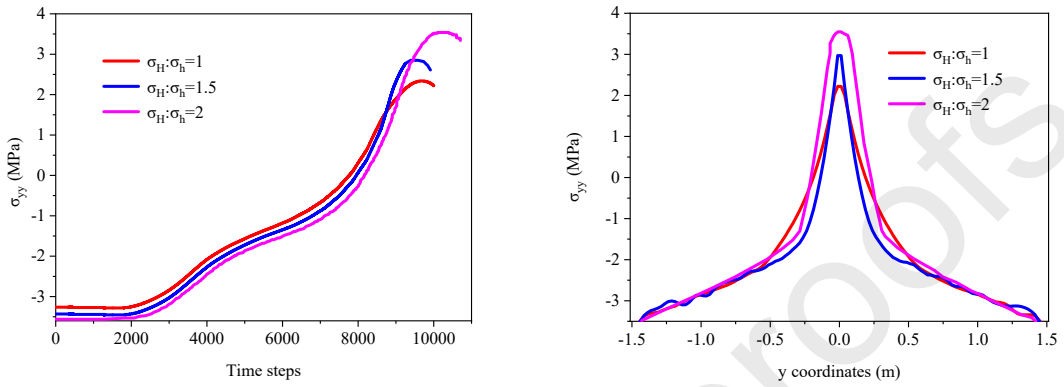

(a) (b)

Fig. 9. The influence of in-situ stress ratio on the distribution of tensile stress on the right side of the HF: (a) the curve of tensile stress at point A (when the value reaches its peak); (b) the distribution of tensile stress on the right side of the NF.

Combined with the contents of sections 4.1 and 4.2, following the model shown in Fig. 10 and resetting the boundary conditions, the interaction results of HF and NF under different in-situ stress ratios and friction coefficients are obtained by fixing σ_h to 6 MPa and adjusting σ_H and μ_{fri}. The numerical simulation results are compared with the prediction results of the RP criterion (as shown in Equation (15), the compressive stress is negative. T_0 is the tensile strength of the rock, and in PD, T_0 can be related to the critical elongation of the bond[63]). The simulation results of this model are consistent with the prediction results of the RP criterion[64] (Fig. 10).

$$\frac{-\sigma'_{xx}}{T_0-\sigma'_{yy}} > \frac{0.35+\frac{0.35}{\mu_{fri}}}{1.06} \tag{15}$$

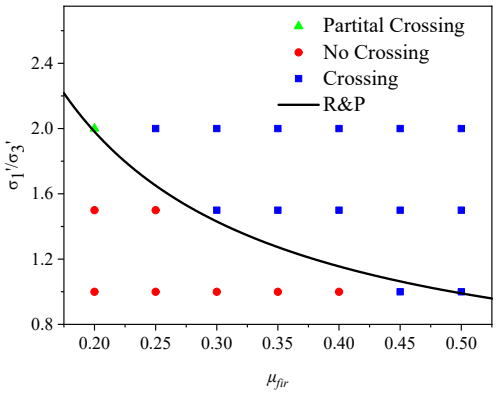

Fig. 10. Comparison of numerical results and R&P criteria on prediction results.

3.3. Effect of fracturing fluid viscosity

Case C illustrates the effect of fracturing fluid viscosity on the interaction between the HF and the NF. The fracturing fluid viscosity affects the flow velocity and pressure distribution of the fracturing fluid in the fractures. With the increase in the viscosity of the fracturing fluid, the fracturing process changes from "toughness dominated" to "viscosity dominated"[65]. At this time, the propagation speed and opening degree of HF are decelerated. This observation can be explained by the fact that the speed of the fracturing fluid entering the NF decreased.

Under different fracturing fluid viscosities, when HF propagates toward the point A (1000 steps after the HF reaches point A), the numerical results are given in Fig. 11.

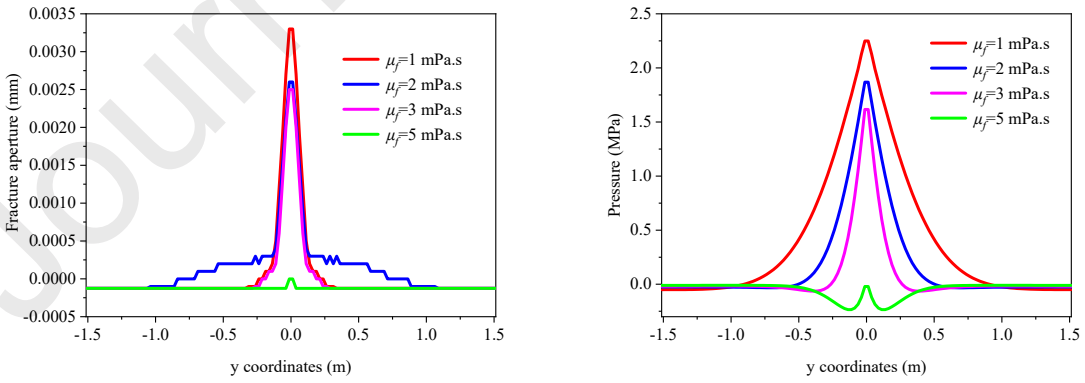

(a) (b)

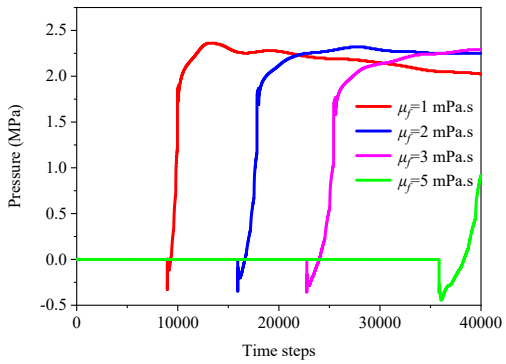

(c)

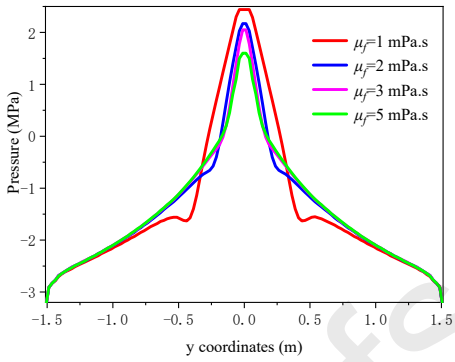

(d)

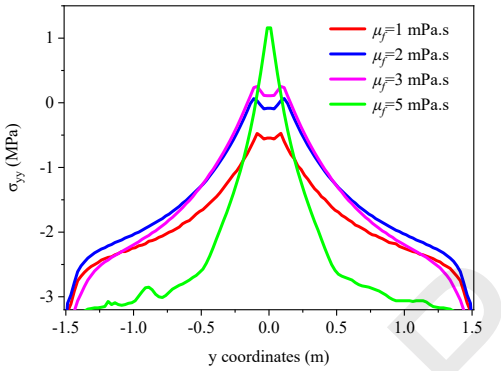

(e)

Fig. 11. Influence of fracturing fluid viscosity on the interaction between HF and NF: (a) aperture distribution of NF; (b) pressure distribution in the NF; (c) curve of tensile stress change at point B; (d) tensile stress distribution on the surface of NF (when the value reaches its peak); (e) tensile stress distribution on the surface of NF (5000 steps after the HF come into contact with NF).

According to the calculation results, with the increase in fracturing fluid viscosity, the speed of the fracturing fluid entering the NF decreases significantly (as shown in Fig. 11(c). When μ_f=5 mPa·s, the fracturing fluid could not completely fill the newly expanded space in the NF, so negative pressure arises in the NF), and the HF aperture also decreases significantly (Fig. 11(a)). Although the peak friction on the right side of the NF (at point B) decreases slightly with the increase in fracturing fluid viscosity (Fig. 11(d)), the period during which friction is maintained at a high value is significantly prolonged (Fig. 11(c) and (e); after 5000 steps of the HF propagating to point A, the tensile stress acting on the right side of the NF is much greater when μ_f is 5mPa·s than when u_f is 1mPa·s). Therefore, the higher the fracturing fluid viscosity, the more favorable it is for the HF to penetrate the NF. This conclusion is consistent with that obtained by Llanos et al[6].

3.4. Effect of injection rate

Case D illustrates the effect of the injection rate on the interaction between HF and NF. With the increase in the injection rate of the fracturing fluid, the HF propagation tends to be "toughness dominated". The injection rate affects the propagation and opening rate of the HF, as well as the opening rate of NF. Therefore, the injection rate also affects the interaction between NF and HF. Fig.12(a) shows the change curve of the tensile stress at point B of NF surface for different injection rates; similarly, Fig. 12(b) shows the change curve of the fracturing fluid pressure in the NF near point B, and Fig.12(c) reflects the change curve of the aperture of the NF near point B.

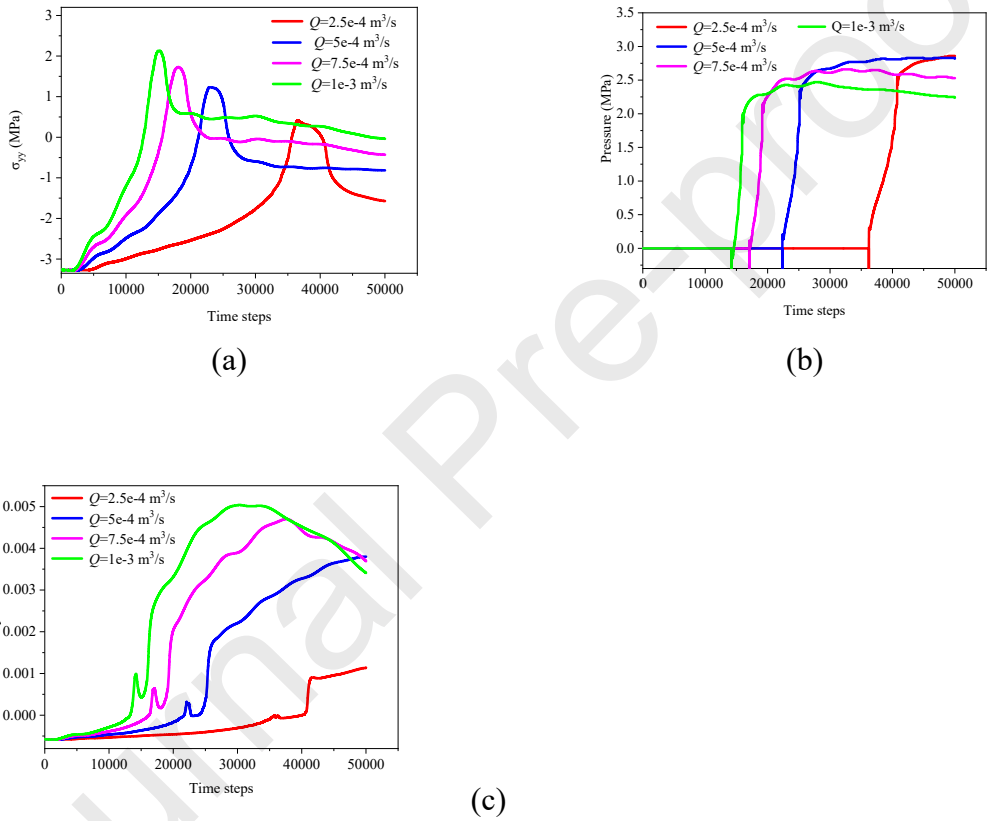

Fig. 12. The influence of the fracturing fluid injection rate on the interaction between HF and NF: (a) variation in the tensile stress at point B; (b) the pressure curve in the NF near point B; (c) variation in the tensile stress at point B.

Fig. 12 shows that with the increase injection rate, although the increase in the opening rate of NF (Figs. 12(b) and (c)) leads to the decrease in the period of high friction force of the rock mass on the right side of NF (Fig. 12(a)), the increase in injection rate can significantly increase the friction force of the rock mass on the right side of the NF (Fig. 12(a)). Therefore, at higher injection rates, the rock mass on the right side of NF is more likely to crack, and HF is more likely to penetrate NF.

3.5. Effect of approach angle

To study the effect of the approach angle on the interaction between a HF and a NF, a new hydraulic fracturing model is established, as shown in Fig. 13. The model size and material parameters are the same as those in sections 4.1 to 4.4, and an inclined cohesive joint is arranged in the model. The cohesive joint model can be referred to in our published works[52]. The parameters and loading conditions of the model are shown in Table 3. The emphasis here is that, to simulate real conditions as closely as possible, the joint in this section is a cohesive fracture before opening (reference can be made to our published work on the cohesive fracture PD model[52]). When the cohesive fails and the joint opens, the frictional force and contact force on the fracture surface come into effect.

Table 3 Loading conditions and model parameters.

Approach angle θ	Minimum horizontal stress σ_h	Maximum horizontal stress σ_H	Friction coefficient μ_{fir}	Fracturing fluid viscosity μ_f	Injection rate Q
15-90°	10 MPa	12.5 MPa	0.6	15e-3 Pa·s	1e-3 m^3/s

Fracture energy of the rock G_{c1}	Fracture energy of the joint G_{c2}
100 J/m^2	20 J/m^2

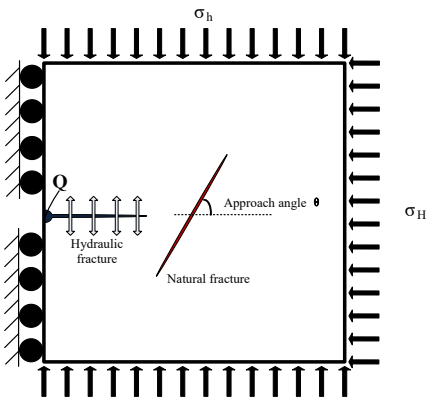

Fig. 13. Diagram of the model with a cohesive joint.

Because the NF is inclined, the rock mass on the right side of the NF is damaged by not only tension but also the combined action of tension and shear. The failure mechanism is complex, so it is not convenient to analyze the interaction between HF and NF by comparing the stress distribution on the right side of the NF. When NF is inclined, it is difficult to predict the position where NF will be penetrated by HF as HF may not propagate along a straight line. Therefore, it is difficult to analyze the influence of the approach angle on the interaction between the HF and the NF by directly presenting the aperture and pressure distribution of the NF. Therefore, the fracture propagation path and distribution will be studied to analyze the interaction between NF and HF under different approach angles. The results of fracture distribution at different approach angles are shown in Fig. 14, and the evolution of fracture length is shown in Fig. 15.

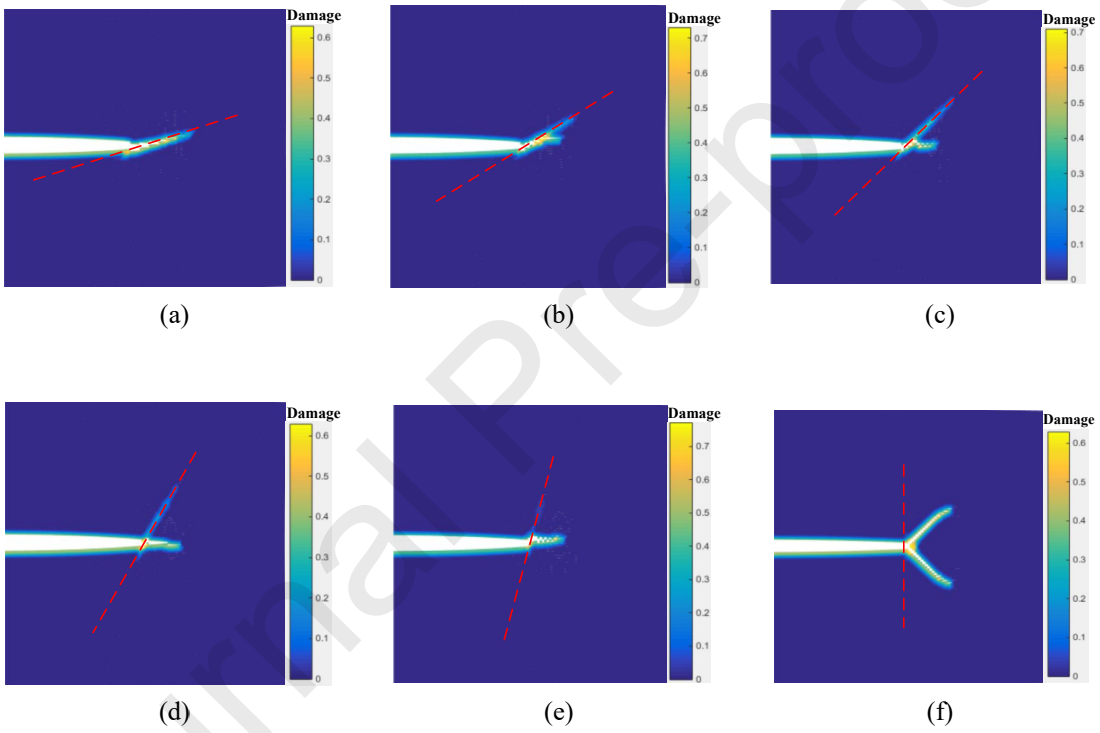

Fig. 14. Fracture distribution in the case with different inclination angle of NF: (a) θ=15°;(b) θ=30°; (c) θ=45°; (d) θ=60°; (e) θ=75°; (f) θ=90°.

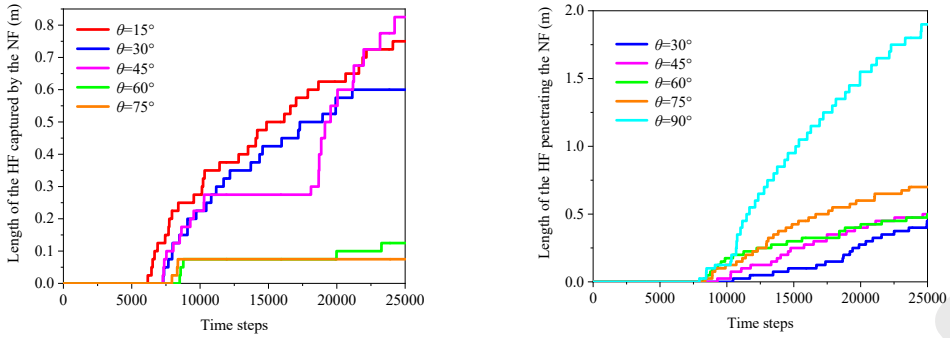

(a) (b)

Fig. 15. Evolution of fracture length: (a) length of the HF captured by the NF; (b) length of the HF captured by the NF.

According to the simulation results, when the dip angle of NF is below 30°, HF is completely captured by NF (Fig. 14(a)). When the dip angle of NF is between 30° and 60°, HF bifurcates near NF: one branch being captured by the NF and the other one penetrating it. Moreover, one observes that the propagation speed of HF increases with the increase in the dip angle of NF (Fig. 15). When the dip angle of NF is 75° or more, HF penetrates NF without capture. When the dip angle of HF is approximately 75°, it deviates slightly before penetrating NF (Fig. 14(e)). Whereas, when the angle is 90°, HF bifurcates and traverses NF (both bifurcations directly penetrate the interface, as shown in Fig.14(f)). The simulated bifurcation of fracture, while penetrating a weakly adhesive interface, mirrors a previously verified experiment. This phenomenon is coherent with the experimental data of [66], which is worthy of further investigation. The simulation results also reveal a significant influence pattern of HF and the morphology and propagation mode of the NF: when HF interacts with NF (e.g. HF capture or deviation along NF), HF propagation slows while the aperture widens. If HF directly penetrates the interface, it propagates faster, but with a lower aperture (compare Fig. 14(f) with other images in Fig. 14, as well as compare the light blue curve in Fig. 15(b) with other curves).

4. Interaction patterns between a HF and a NF in three-dimensional rocks

In the previous section, the interaction mechanisms between HF and NF have been analyzed under 2D conditions. Additionally, the influencing factors, such as the stress distribution, fracture surface friction coefficients, and hydraulic fracturing construction parameters, on the interaction between HF and NF are investigated. However, in actual hydraulic fracturing operations, both HFs and NFs present as complex discontinuity in three-dimensional space[67]. In addition, the fracture propagation depends on the in-situ triaxial stress field[52]. Although two-dimensional hydraulic fracturing models are capable of revealing the principal interaction

mechanisms between NF and HF, the propagation patterns of fracture surfaces cannot be captured by them. Another noteworthy point is that, based on the two-dimensional model, researchers[68] have classified the interaction patterns between HF and NF as penetration, deflection, and captured, et. Under three-dimensional conditions, "diversion" is also identified as a significant interaction pattern (as shown in Fig. 16), wherein HF bypasses NF and continues to propagate without penetration[69].This particular interaction pattern can only be simulated using a three-dimensional model. In this section, the interaction patterns between HFs and NFs under three-dimensional conditions are investigated, as well as the propagation modes and distribution characteristics of fracture surfaces.

The model's dimensions are 1.05 m*1.05 m*1.8 m. The elastic modulus of the studied material E is 15 GPa, and the critical energy release rate G_c is 100 J/m^2. The characteristic length of material points Δx is 0.03 m, and the time step Δt used in the calculations is 2.5e-5 s. The injection rate of the fracturing fluid is 2e-4 m^3/s.

For the convenience of studying the interaction morphology between HF and NF in 3D, their relative positional relationships will be categorized into x-z oblique intersection (NF's outward normal parallel to the x-z plane), y-z oblique intersection (NF's outward normal parallel to the y-z plane), and x-y oblique intersection (NF's outward normal parallel to the x-y plane).

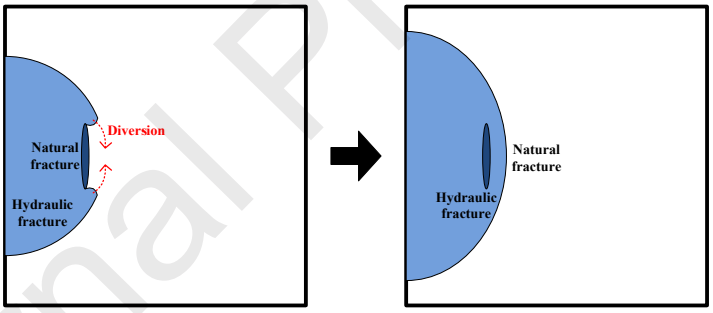

Fig. 16. Diagram of the HF bypassing the NF.

4.1. The x-z oblique intersection

The "x-z oblique intersection" refers to the situation where the outer normal of NF is parallel to the x-z plane (Fig. 17). This case is similar to a two-dimensional model, which has been studied in previous section. Different interaction modes between HF and NF can be obtained by adjusting in-situ stress distribution (σ_x, σ_y, and σ_z), fracturing fluid viscosity μ_f, and NF dip angle θ. The boundary conditions and construction parameters for each group of cases are given in Table 4.

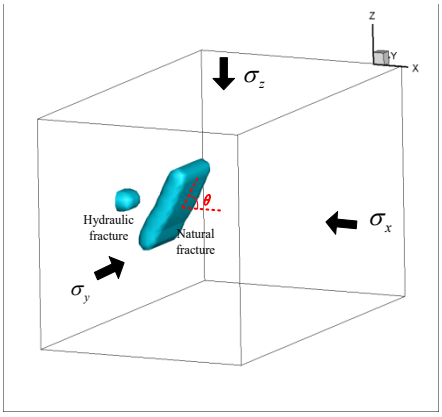

Fig. 17. Diagram of the x-z oblique intersection.

Table 4 Boundary conditions and construction parameters of the x-z oblique intersection model.

Case	Horizontal stress σ_x	Horizontal stress σ_y	Vertical stress σ_z	Friction coefficient μ_{fir}	Fracturing fluid viscosity μ_f	θ
A	10 MPa	10 MPa	10 MPa	0.45	10 mPa·s	60°
B	10 MPa	10 MPa	10 MPa	0.45	60 mPa·s	60°
C	10 MPa	30 MPa	10 MPa	0.45	10 mPa·s	60°
D	10 MPa	10 MPa	10 MPa	0.45	10 mPa·s	75°
E	20 MPa	10 MPa	10 MPa	0.45	10 mPa·s	75°

The injection volume of fracturing fluid pump Q_v is approximately 2.5e-5 m^3 in each case (Fig. 18). The simulation results indicate that the "capture" state in the 3D (Fig. 18(a)) differs significantly from those in 2D[68, 70]. In 3D model, the edges of HF and NF come into contact and fuse, resulting in the upper end of the NF forming a shape resembling a "sunshade" (i.e., after HF is captured by NF, NF not only propagates in the x-direction but also extends in the x-z plane). In Case B, the increased viscosity of the fracturing fluid (μ_f=60 mPa·s) leads to a reduced rate of fluid influx into NF, limiting the opening of NF and thereby promoting HF to bypass it. As revealed in our previous research[50], an increase in horizontal stress along the y-direction can promote the propagation of HF in the perpendicular direction (x-direction). Therefore, in the Case C, with the increasing of σ_y, HF not only penetrates NF but also bypass the NF, propagating on the other side of NF (as shown

in Fig. 18(d)). In the Case D, despite having construction parameters and boundary conditions identical to Case A, the increased dip angle (θ=60° in case A, while θ=60° in case D) of NF induces HF to bypass it. Therefore, with the growing inclination angle, the diversion occurrence becomes more likely (comparing Fig. 18(f) to Fig. 18(a)). Furthermore, although HF bypasses NF in both Case B and Case D, in the scenario with a smaller dip angle (Case B), there is also lateral displacement of HF during bypassing. In other words, the simulation results of the Case B exhibit a mixed form of bypassing and deflection. The Case E (Figs. 18(g) and (h)) further validates the conclusions from Section 4. These observations indicate the horizontal stress increases, the frictional forces acting on the surface of NF also increase and then facilitatesthe penetration of HF through NF. In this particular case, due to the incline of NF, there is also lateral displacement of HF as it penetrates NF, resulting in an arched distribution of HF on the other side of NF. The obtained results further indicate that, despite the distribution pattern of fractures in 2D closely resembling the x-z intersection, the 3D model is still capable of reproducing numerically a more diverse and accurate pattern of fracture propagation.

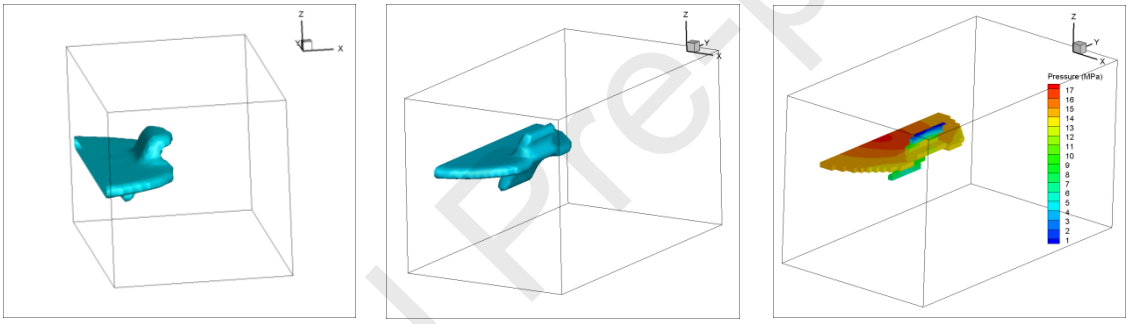

(a) (b) (c)

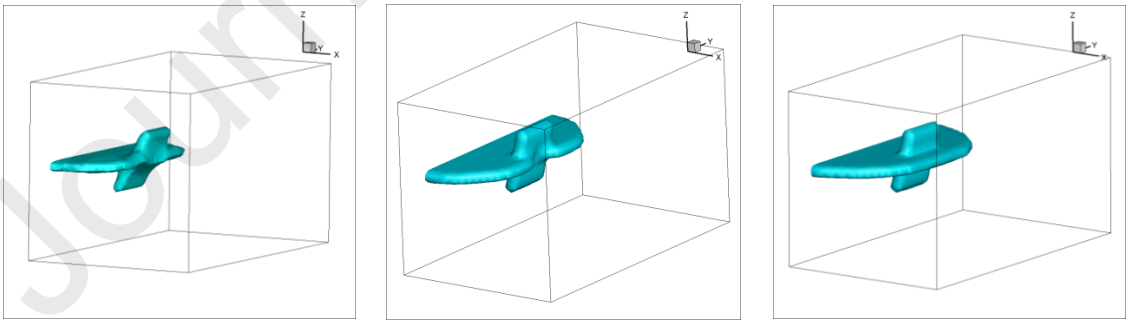

(d) (e) (f)

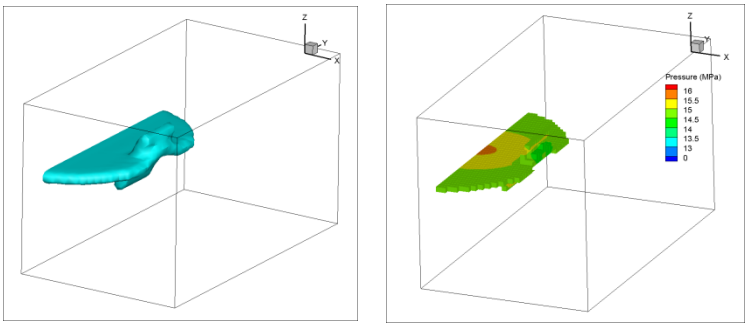

(g) (h)

Fig. 18. Fracture distribution of different cases in x-z oblique intersection: (a) case A; (b) case B; (d) case C; (e) case D (Q_v= 2.25 m^3); (f) case D (Q_v= 2.25 m^3); (g) case E; and fracturing fluid pressure distribution of case B (C) and case E (h).

Furthermore, the three-dimensional model's capacity to accurately simulate the propagation of HF in the height (or width) direction presents a challenge for NF propagation once it intersects with HF. This presents a notable deviation from the assumption made in 2D, where fractures are typically assumed to extend infinitely in the height direction. This phenomena has been discussed in our previous studies[50].

4.2. The x-y oblique intersection

The "x-y oblique intersection" refers to the crack distribution pattern when the external normal of HF is parallel to the x-y plane, which cannot be studied in a two-dimensional model. Table 5 lists the boundary conditions and construction parameters for each group of cases. The angle between HF and the y-z plane is 25°. The remaining fundamental parameters of the numerical model in this section are consistent with those outlined in Section 5.1.

Table 5 Boundary conditions and construction parameters of the x-y oblique intersection model.

Case	Horizontal stress σ_x	Horizontal stress σ_y	Vertical stress σ_z	Friction coefficient μ_{fir}	Fracturing fluid viscosity μ_f	Length of the NF L
F	15 MPa	10 MPa	10 MPa	0.45	10 mPa·s	0.6 m
G	15 MPa	10 MPa	10 MPa	0.6	10 mPa·s	0.6 m
H	15 MPa	10 MPa	10 MPa	0.45	50 mPa·s	0.6 m

I	15 MPa	10 MPa	10 MPa	0.45	10 mPa·s	0.3 m

The simulation results of the fracture distribution and fracturing fluid pressure distribution when the injection volume of fracturing fluid pump Q_v is approximately 2e-5m^3 are shown in Fig. 19. In Case F, HF is entirely captured by NF, incapable of penetrating or bypassing it (Fig. 19(a)). Conversely, in Case I, due to the halving of the NF's length compared to that in Case F, the HF bypasses the NF (Fig. 19(g)). Hence, the length of the NF significantly influences the HF's ability to bypass it. In Case G, due to the increased friction coefficient of the fracture surface, HF penetrated NF. In contrast, in Case H, the elevated fracturing fluid viscosity restricted the rate of pressure increase within NF (Fig. 19(f)), consequently limiting the opening speed of NF. This restriction facilitated HF penetration through NF, while simultaneously giving rise to the phenomenon of HF bypassing NF (Fig. 19(e)), thus a mixed propagation form involving both penetration and circumvention occurs in Case H. This also results in the boundary of HF in Case H being closer to a smooth arc compared to that in Case G.

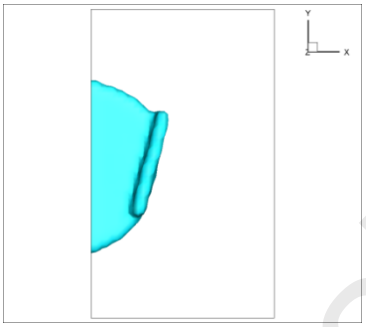

(a)

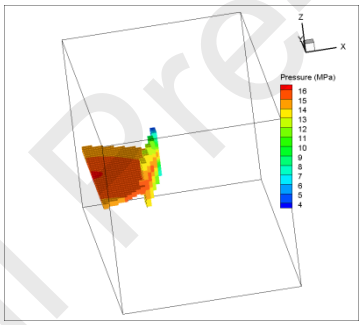

(b)

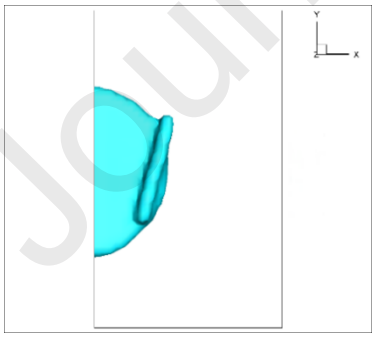

(c)

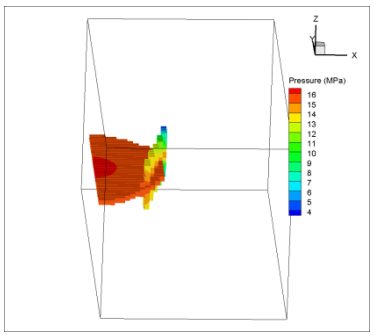

(d)

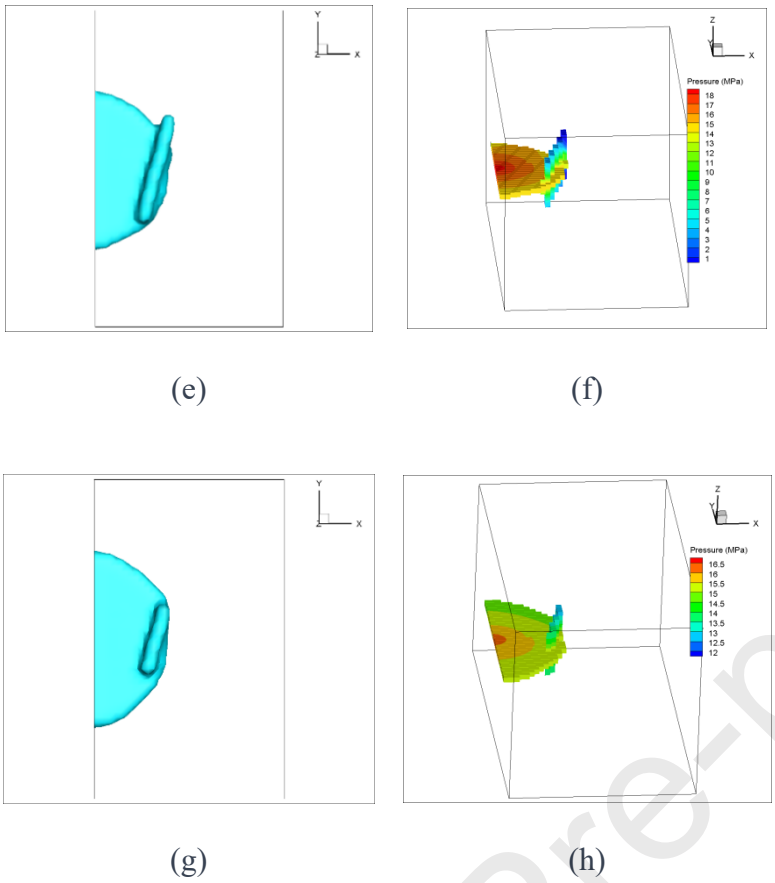

(e) (f)

(g) (h)

Fig. 19. Simulation results of the x-y oblique intersection: (a) fracture distribution of case F; (b) fracturing fluid pressure distribution of case F; (c) fracture distribution of case G; (d) fracturing fluid pressure distribution of case G; (e) fracture distribution of case H; (f) fracturing fluid pressure distribution of case H; (g) fracture distribution of case I; (h) fracturing fluid pressure distribution of case I.

4.3. The y-z oblique intersection

The "x-y oblique intersection" refers to the crack distribution pattern when the external normal of HF is parallel to the x-y plane, which cannot be studied using a 2D model. The used boundary conditions and model parameters are listed in Table 6, where θ represents the angle between NF and the x-y plane. In this section, the friction coefficient μ_{fri} is 0.3, the fracturing fluid viscosity μ_f is 10 mPa·s. In cases J, K, and L, the angle between the hydraulic fractures (HF) and the x-y plane is 90°, which represents a special fracture distribution pattern known as "orthogonal".

When the NF is parallel to the y-z plane, HF does not penetrate NF, and the propagation pattern of HF is a combination of "capture" and "diversion". Whether NF can separate the influx of fracturing fluid and expand is the focal point of this section. Therefore, the friction coefficient and fracturing fluid viscosity are fixed in this set of cases (these two parameters mainly affect the penetration of the HF), and different fracture propagation patterns are obtained by adjusting the in-situ stress distribution.

Table 6 Boundary conditions of the y-z oblique intersection model.

Case	Horizontal stress σ_x	Horizontal stress σ_y	Vertical stress σ_z	θ
J	10 MPa	10 MPa	10 MPa	90°
K	10 MPa	5 MPa	10 MPa	90°
L	10 MPa	10 MPa	20 MPa	90°
M	10 MPa	10 MPa	15 MPa	45°
N	10 MPa	5 MPa	10 MPa	45°

Fig. 20 shows the simulation results of the distribution of fracture and fluid pressure of cases J to N. During hydraulic fracturing, the HF are only likely to propagate when the fracturing fluid pressure is roughly not lower than the sum of the normal stress on the fracture plane and the tensile strength of the rock. This also explains one of the influencing mechanisms in the propagation of HFs and NFs concerning the distribution of in-situ stress. In case J, the normal stress acting on the HF (σ_z=10 MPa) is equal to the normal stress acting on the HF (σ_y=10 MPa). Additionally, due to the viscosity of the fracturing fluid (resulting in higher fracturing fluid pressure near the wellbore compared to the far end), the fracturing fluid pressure within the NF does not meet the conditions (as described above) required to sustain the expansion of the natural fractures (as shown in Fig. 20(c)). Therefore, the NF in case J dose not open or propagate (Figs. 20(a) and (b)). In case K, the normal stress acting on the HF is significantly higher than the normal stress acting on the HF. Therefore, the pressure of the fracturing fluid flowing from HF into NF is sufficient to cause the NF to open and propagate (Fig. 20(d)). In case L, due to the significant increase in vertical in-situ stress (σ_z=20 MPa) compared to horizontal in-situ stress (σ_x=σ_y=20 MPa), the HF bifurcates and propagates in the vertical direction (Fig. 20(e)). This is in line with the theory that the HF propagates parallel to the maximum principal stress direction. Based on the simulation results of the two-dimensional model, we preliminarily believe that when the ratio of the difference between vertical in-situ stress and rock tensile strength to horizontal in-situ stress is higher than a certain critical value, HF will bifurcate and deflect towards the vertical direction. The mechanism by which the originally horizontally distributed HF bifurcates and deflects to the vertical direction is still worth further discussion in the future. In cases M and N, the normal stress acting on the HF (σ_z) is significantly greater than that acting on the NF (σ_y*cosθ+σ_z*sinθ), resulting in the NF opening and propagating. In case M,

where $\sigma_y=\sigma_z$, the NF does not deflect but rather propagate within their respective plane. On the other hand, in case N, where σ_z is greater than σ_y, the net force experiences deflection and propagate within the x-z plane. Due to the significantly smaller difference between the normal stresses acting on the HF surface and NF surface in Case M (σ_z-(σ_y*cosθ+σ_z*sinθ)) compared to the difference in Case N (σ_z-σ_y), the propagation rate of the HF in Case M is noticeably greater than that in Case N. Conversely, the propagation rate of the NF in Case M is significantly slower than that in Case N.

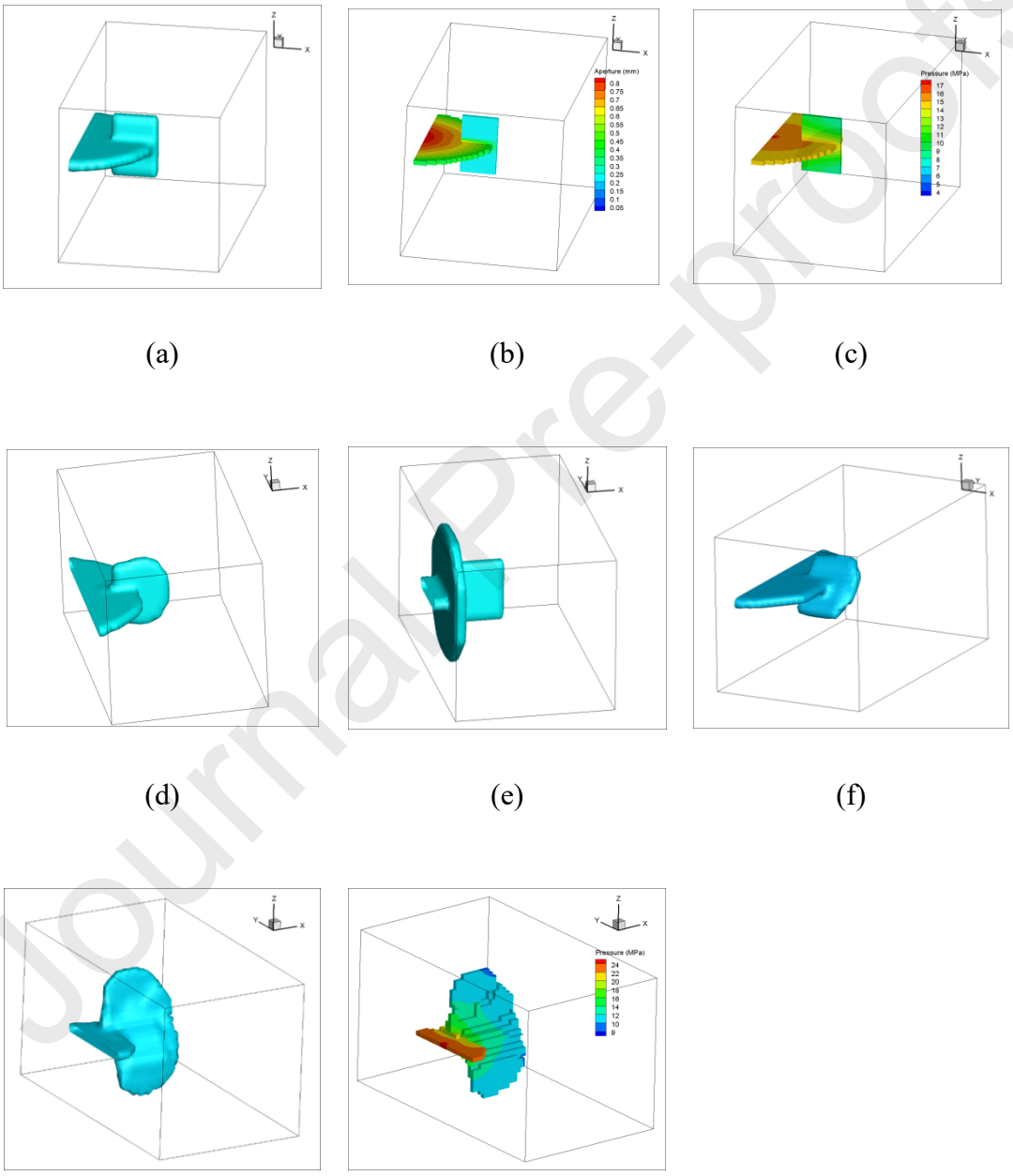

(a) (b) (c)

(d) (e) (f)

(g) (h)

Fig. 20. Simulation results of the x-y oblique intersection: (a) fracture distribution of

case J; (b) fracture aperture distribution of case J; (c) fracture fluid pressure distribution of case J; (d) fracture distribution of case K; (e) fracture distribution of case L; (f) fracture distribution of case M; (g) fracture distribution of case N; (h) fracture fluid pressure distribution of case N.

5. Numerical simulation of hydraulic fracturing in a jointed rock mass

Based on the careful investigation of the interaction mechanisms between HF and a single NF, as well as the morphology of fracture propagation mentioned earlier, this section conducts simulations of hydraulic fracturing in reservoirs containing fractures with arbitrary distributions. Despite a significant amount of numerical research published on hydraulic fracturing in fractured rock formations, much of it has been based on two-dimensional models or pseudo-three-dimensional (P3D) models. As revealed in this work, the interaction between HFs and NFs are challenging to analyze using two-dimensional models. Therefore, it is a needed to develop more sophisticated true-three-dimensional models to simulate the hydraulic fracturing of jointed rocks.

A three-dimensional jointed rock model, as shown in Fig. 21, has been constructed with dimensions of 1.8m*1.8m*1.05m. The elastic modulus of the rock E is 15 GPa, and the critical energy release rate for the rock G_c is 100 J/m^2. The characteristic length of material points Δx is 0.03 m, and the time step Δt used in the calculations is 2.5e-5 s. The injection rate of the fracturing fluid is 2e-4 m^3/s. The boundary conditions and model parameters are listed in Table 7, where θ represents the angle between the NF and the x-y plane.

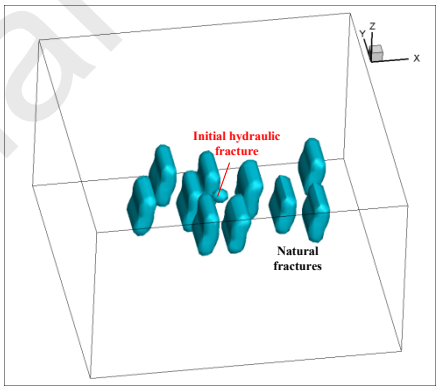

Fig. 21. 3D fractured rock mass model diagram

Table 7 Boundary conditions and construction parameters of the jointed rock model.

Case	Horizontal stress σ_x	Horizontal stress σ_y	Vertical stress σ_z	Friction coefficient μ_{fri}	Fluid viscosity μ_{fri}	θ

A	10 MPa	10 MPa	10 MPa	0.45	15 mPa·s	60°
B	20 MPa	10 MPa	10 MPa	0.45	15 mPa·s	60°
C	20 MPa	10 MPa	10 MPa	0.8	15 mPa·s	60°
D	20 MPa	10 MPa	10 MPa	0.8	50 mPa·s	60°
E	10 MPa	10 MPa	10 MPa	0.45	15 mPa·s	75°
F	20 MPa	10 MPa	10 MPa	0.8	15 mPa·s	75°

Fig. 22 shows the simulation results of hydraulic fracturing in jointed rock when the injection volume Qv is about 1e-4 m^3. In Cases A and E, the vertical and horizontal stresses are equal. Therefore, after being captured by the nearest NF, the HF primarily propagates within the plane where the NF is located, rather than continuing to propagate within the horizontal plane. Therefore, when the difference in in-situ stresses is small, NFs will significantly deflect the propagation direction of HF and restrict the propagation of HF in the length direction. When the difference between vertical stress and horizontal stress reaches 10 MPa (case B), the HF will penetrate or bypass the NF and mainly propagate in the x-y plane (as shown in Figs. 22(c) and (d)). As the fracturing fluid viscosity further increases (μ_f=50 mPa·s), the surface of the HF becomes smoother, indicating that the HF tends to propagate more within the x-y plane. On the basis of the construction parameters and boundary conditions in Case B, increasing the dip angle of NFs to 75 °, it is obvious that the HF has a faster propagation rate in the x-y plane, which also verifies an obvious rule that a larger approaching angle is more conducive to HF penetrating NF.

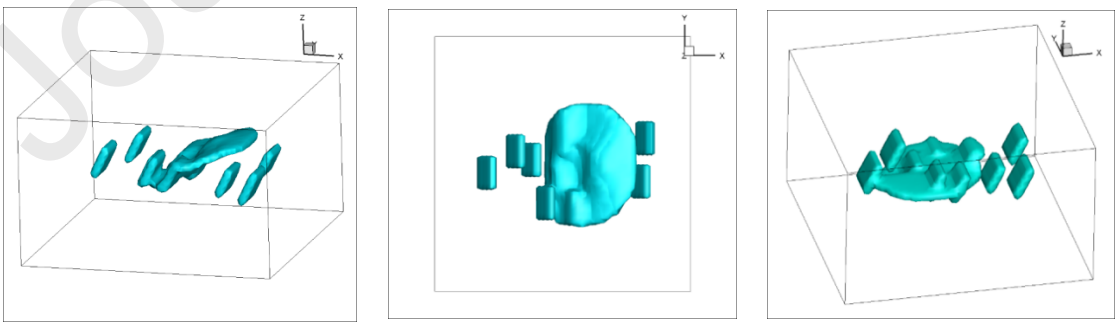

(a) (b) (c)

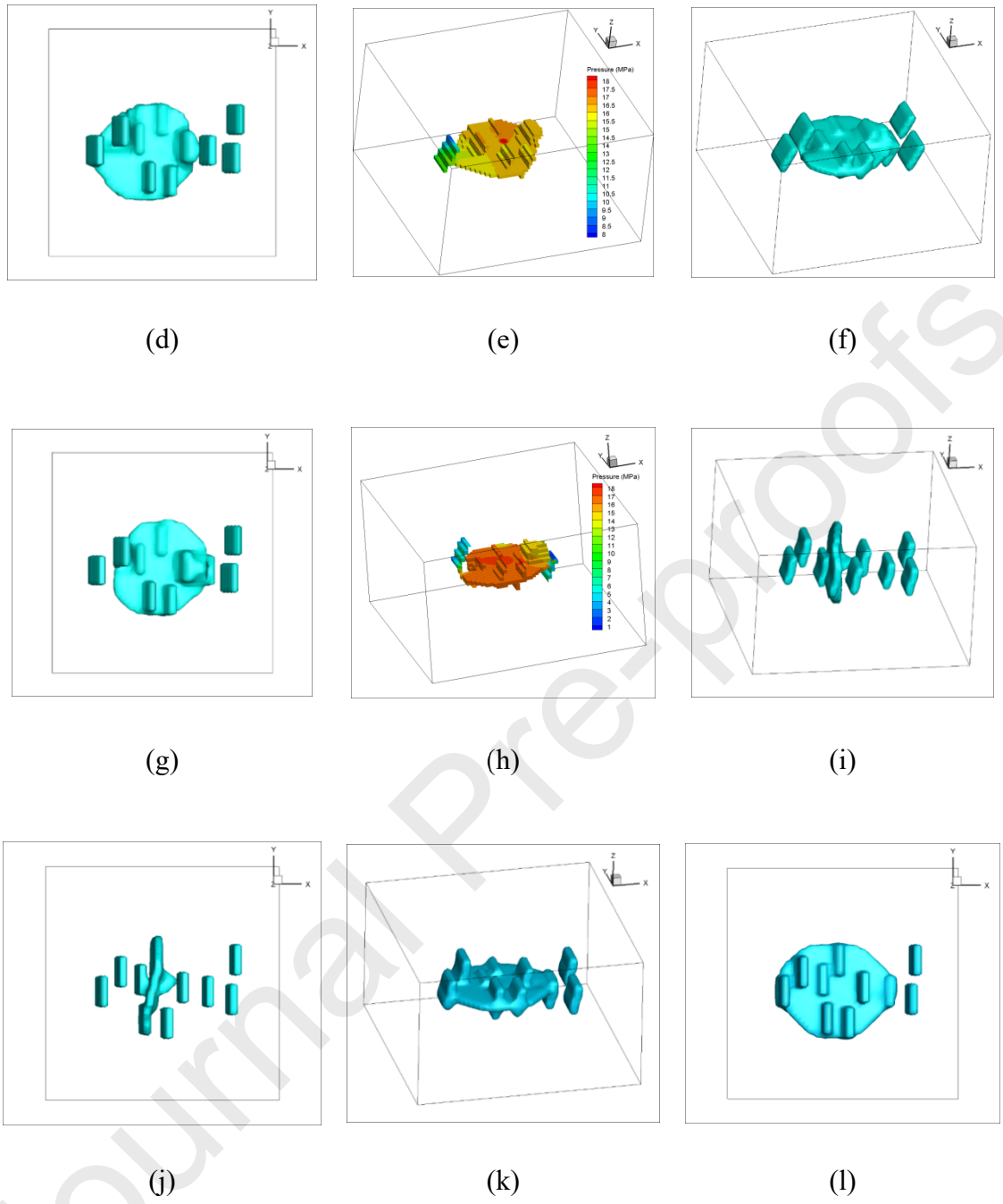

672 **Fig. 22.** Simulation results of hydraulic fracturing in a jointed rock mass: (a) fracture
673 distribution of case A (Qv=0.5e-4 m^3); (b) the projection of fractures in the x-y plane
674 of Case A (Qv=0.5e-4 m^3); (c) fracture distribution of case B; (d) the projection of
675 fractures in the x-y plane of Case B; (e) fluid pressure distribution of case C; (f)
676 fracture distribution of case C; (g) fracture distribution of case D; (h) the projection of
677 fractures in the x-y plane of Case D; (i) fracture distribution of case E (Qv=0.5e-4
678 m^3); (j) the projection of fractures in the x-y plane in Case E (Qv=0.5e-4 m^3); (k)
679 fracture distribution of case F; (l) the projection of fractures in the x-y plane in Case
680 F.

6. Conclusions and discussions

In this article, a self-developed 2D/3D hydraulic fracturing model for fractured rock masses is constructed and used to study the mechanism of fracture interaction and the morphology of fracture propagation in hydraulic fracturing of jointed rock masses. The main research conclusions of this article are as follows:

(1) Based on the two-dimensional numerical model, we clearly illustrated the influence of the in-situ stress ratio, fracture surface friction coefficient, fracturing fluid viscosity, injection rate and fracture dip angle (approach angle) on the interaction between HFs and NFs. The results show that the greater the in-situ stress ratio, the greater the friction coefficient on the NF surface is, and the more likely the HF penetrates the NF. The simulation results closely align with predictions based on the RP criterion[64] and are also consistent with the conclusions obtained by Zhou et al.[68] through numerical simulations. With the increase in fracturing fluid viscosity, the rate of fracturing fluid entering a NF decreases, and the rate of pressure rise in the NF also decreases. At this time, the action time of tensile stress on the NF surface is prolonged, which is more conducive for the HF to penetrate the NF. The numerical research results on the effect of fracturing fluid viscosity on the interaction between HF and NF are consistent with the experimental ones of Llanos et al[6]. A higher injection rate is beneficial to increase the peak tensile stress on the surface of the NF, which is also conducive for the HF to penetrate the NF. As the dip angle of the NF increases, the HF undergoes a sequence of propagation modes, including complete captured, bifurcation and penetration, deviation and penetration, and complete penetration (possibly with bifurcation). Compared to the scenario where the HF directly penetrates the NF, the interaction between the HF and the NF significantly restricts the propagation velocity of the HF and increases the aperture of the HF, which is consistent with the conclusion obtained by Zhang et al.[35] through numerical simulation.

(2) The subsequent study focused on the interaction morphology between the HF and the NF in three-dimensional rocks. The simulation results indicate that “diversion” is an important interaction mode between the HF and the NF in three-dimensional rocks. Larger dip angle of the NF and higher fracturing fluid viscosity are beneficial for the HF to bypass the NF, and this interaction mode cannot be simulated using two-dimensional models. The simulation results of the 3D model also indicate that there exists a mixed interaction mode of penetration and diversion when the length of the NF is limited and the angle between the NF and the HF is less than 90°. The fracturing fluid will preferentially flow into the fracture with the lowest sum of normal stress and rock tensile strength. Only when the normal stress acting on the surface of the HF is significantly greater than the normal stress on the surface of the NF can the NF propagate.

(3) Simulation results of hydraulic fracturing in three-dimensional fractured rock masses indicate that larger horizontal stress differentials, higher fracturing fluid

722 viscosity, and greater dip angle of NFs are favorable for the horizontal propagation of
723 the HF within the horizontal plane, reducing HF roughness. When the horizontal
724 stress differential is relatively small, the HF may be captured by NFs, altering the
725 propagation direction and causing propagation in the vertical direction. The
726 simulation results are similar to the conclusions drawn by Beugelsdijk et al.[71], as
727 well as Fan and Zhang[72] from the experiment.

728 **Acknowledgements**

729 The authors gratefully acknowledge the support of the National Natural Science
730 Foundation of China (Grant Nos. U22A20595, 12202463, 52108366).

731 **References**

732 [1] Warpinski NR, Teufel LW. Influence of geologic discontinuities on hydraulic
733 fracture propagation. Journal of Petroleum Technology. 1987,39:209-220.

734 [2] Blanton TL. An experimental study of Interaction between hydraulically induced
735 and pre-Existing fractures. SPE. 1982.

736 [3] Blanton TL. Propagation of hydraulically and dynamically induced fractures in
737 naturally fractured reservoirs. SPE Unconventional Resources Conference/Gas
738 Technology Symposium: SPE, 1986.

739 [4] Bunger AP, Kear J, Jeffrey RG, et al. Investigation of hydraulic fracture growth
740 through weak discontinuities with active ultrasound monitoring. ISRM Congress:
741 ISRM, 2015.

742 [5] Beugelsdijk LJL, Pater C, Sato K. Experimental hydraulic fracture propagation in
743 a multi-fractured medium. SPE Asia Pacific Conference on Integrated Modelling for
744 Asset Management: SPE, 2000.

745 [6] Llanos EM, Jeffrey RG, Hillis R, et al. Hydraulic fracture propagation through an
746 orthogonal discontinuity: a laboratory, analytical and numerical study. Rock
747 Mechanics and Rock Engineering. 2017,50:2101–2118.

748 [7] Guo TK, Zhang SC, Qu ZQ, et al. Experimental study of hydraulic fracturing for
749 shale by stimulated reservoir volume. Fuel. 2014,128:373-380.

750 [8] Hanson ME, Anderson GD, Shaffer RJ, et al. Some Effects of Stress, Friction, and
751 Fluid Flow on Hydraulic Fracturing. Society of Petroleum Engineers Journal.
752 1982,22:321-332.

753 [9] Hanson ME, Shaffer RJ, Anderson GD. Effects of various parameters on hydraulic
754 fracturing geometry. Society of Petroleum Engineers Journal. 1981,21:435-443.

755 [10] Pippan R, Flechsig K, Riemelmoser FO. Fatigue crack propagation behavior in

the vicinity of an interface between materials with different yield stresses. Materials Science & Engineering A. 2000,283:225-233.

[11] Wang SL, Xing CL, Zhang DS, et al. The Fracture Behavior in the Vicinity of Interface Based on the Digital Speckle Experiment. Spe Asia Pacific Oil & Gas Conference & Exhibition2016.

[12] Warpinski NR, Teufel LW. Influence of Geologic Discontinuities on Hydraulic Fracture Propagation (includes associated papers 17011 and 17074). Journal of Petroleum Technology. 1987,39:209-220.

[13] Renshaw CE, Pollard DD. AN EXPERIMENTALLY VERIFIED CRITERION FOR PROPAGATION ACROSS UNBOUNDED FRICTIONAL INTERFACES IN BRITTLE, LINEAR ELASTIC-MATERIALS. International Journal of Rock Mechanics & Mining Science & Geomechanics Abstracts. 2009,32:237-249.

[14] Gu H, Weng X. Criterion for fractures crossing frictional interfaces at non-orthogonal angles. Us Rock Mechanics Symposium & Us-canada Rock Mechanics Symposium2010.

[15] Sarmadivaleh M, Rasouli V. Modified Reinshaw and Pollard Criteria for a Non-Orthogonal Cohesive Natural Interface Intersected by an Induced Fracture. Rock Mechanics&Rock Engineering. 2014,47:2107-2115.

[16] Anderson GD. Effects of mechanical and frictional rock properties on hydraulic fracture growth near unbonded interfaces. 1979.

[17] Hanson ME, Shaffer RJ, Anderson GD. Effects of various parameters on hydraulic fracturing geometry: Hanson, M E; Shaffer, R J; Anderson, G D Soc Petr Engr J, V21, N4, Aug 1981, P435–443. international journal of rock mechanics & mining sciences & geomechanics abstracts. 1982.

[18] Leguillon D. Strength or toughness? A criterion for crack onset at a notch. European Journal of Mechanics - A/Solids. 2002,21:61-72.

[19] Yew CH, Lodde P. Propagation of a hydraulically induced fracture in layered medium. SPE 11870. 1983.

[20] Cleary MP. Comprehensive design formulae for hydraulic fracturing. SPE Annual Technical Conference and Exhibition: Society of Petroleum Engineers, 1980.

[21] Shi F, Wang X, Liu C, et al. An XFEM-based method with reduction technique for modeling hydraulic fracture propagation in formations containing frictional natural fractures. Engineering Fracture Mechanics. 2017,173:64-90.

[22] Khoei AR, Vahab M, Hirmand M. An enriched–FEM technique for numerical simulation of interacting discontinuities in naturally fractured porous media.

Computer Methods in Applied Mechanics & Engineering. 2017,331:197-231.

[23] Wang XL, Shi F, Liu C, et al. Extended finite element simulation of fracture network propagation in formation containing frictional and cemented natural fractures. Journal of Natural Gas Science and Engineering. 2017:S1875510017304833.

[24] Khoei AR, Hirmand M, Vahab M, et al. An enriched FEM technique for modeling hydraulically driven cohesive fracture propagation in impermeable media with frictional natural faults: Numerical and experimental investigations. International Journal for Numerical Methods in Engineering. 2015,104:439-468.

[25] Cruz F, Roehl D, Vargas E. An XFEM element to model intersections between hydraulic and natural fractures in porous rocks. International Journal of Rock Mechanics and Mining Sciences. 2018,112:385-397.

[26] Khoei AR, Vahab M, Hirmand M. Modeling the interaction between fluid-driven fracture and natural fault using an enriched-FEM technique. International Journal of Fracture. 2015b:1-24.

[27] Yew CH, Chiou YJ. Effects of in-situ stresses and layer properties on the containment of a hydraulic fracture. SPE 12332. 1983.

[28] Cooke ML, Underwood CA. Fracture termination and step-over at bedding interfaces due to frictional slip and interface opening. Journal of Structural Geology. 2001,23:223-238.

[29] Zhang X, Jeffrey RG, Thiercelin M. Deflection and propagation of fluid-driven fractures at frictional bedding interfaces: A numerical investigation. Journal of Structural Geology. 2007,29:396-410.

[30] Zhang X, Jeffrey RG. Reinitiation or termination of fluid-driven fractures at frictional bedding interfaces. Journal of Geophysical Research: Solid Earth. 2008,113:-.

[31] Dong CY, Pater CJD. Numerical implementation of displacement discontinuity method and its application in hydraulic fracturing. Computer Methods in Applied Mechanics & Engineering. 2001,191:745-760.

[32] Akulich AV, Zvyagin AV. Interaction between hydraulic and natural fractures. Fluid Dynamics. 2008,43:428-435.

[33] Abdollahipour A, Marji MF. A thermo-hydromechanical displacement discontinuity method to model fractures in high-pressure, high-temperature environments. Renewable Energy. 2020,153:1488-1503.

[34] Abdollahipour A, Fatehi Marji M, Yarahmadi Bafghi AR, et al. Numerical

826 investigation of effect of crack geometrical parameters on hydraulic fracturing process
827 of hydrocarbon reservoirs. Journal of Mining and Environment. 2016,7:205-214.

828 [35] Zhang X, Jeffrey RG, Thiercelin M. Mechanics of fluid-driven fracture growth in
829 naturally fractured reservoirs with simple network geometries. Journal of Geophysical
830 Research: Solid Earth. 2009,114(B12).

831 [36] Behnia M, Goshtasbi K, Marji MF, et al. Numerical simulation of interaction
832 between hydraulic and natural fractures in discontinuous media. Acta Geotechnica.
833 2015,10:533-546.

834 [37] Moradi M, Tokhmechi B, Rasouli V, et al. A Comprehensive Numerical Study of
835 Hydraulic Fracturing Process and Its Affecting Parameters. Geotechnical and
836 Geological Engineering. 2017,35:1035-1050.

837 [38] Zhang Z, Li X, Yuan W, et al. Numerical analysis on the optimization of
838 hydraulic fracture networks. Energies. 2015,8:12061-12079.

839 [39] García X, Nagel N, Zhang F, et al. Revisiting Vertical Hydraulic Fracture
840 Propagation Through Layered Formations – A Numerical Evaluation. 47th US Rock
841 Mechanics/Geomechanics Symposium2013.

842 [40] Fatahi H, Hossain MM, Sarmadivaleh M. Numerical and experimental
843 investigation of the interaction of natural and propagated hydraulic fracture. Journal
844 of Natural Gas Science and Engineering. 2017,37:409-424.

845 [41] Wasantha P, Konietzky H, Weber F. Geometric nature of hydraulic fracture
846 propagation in naturally-fractured reservoirs. Computers and Geotechnics.
847 2017,83:209-220.

848 [42] Zhang F, Dontsov E, Mack M. Fully coupled simulation of a hydraulic fracture
849 interacting with natural fractures with a hybrid discrete-continuum method.
850 International Journal for Numerical and Analytical Methods in Geomechanics.
851 2017,41:1430-1452.

852 [43] Bakhshi E, Rasouli V, Ghorbani A, et al. Hydraulic Fracture Propagation:
853 Analytical Solutions versus Lattice Simulations. Journal of Mining and Environment.
854 2019,10:451-464.

855 [44] Zhang Z, Ghassemi A. Simulation of hydraulic fracture propagation near a
856 natural fracture using virtual multidimensional internal bonds. International Journal
857 for Numerical and Analytical Methods in Geomechanics. 2015,35:480-495.

858 [45] Zhao HJ, Ma FS, Liu G, et al. Influence of different sacles of structural planes on
859 propagation mechanism of hydraulic fracturing. Journal of Engineering Geology.
860 2016,024:992-1007.

[46] Song CP, Lu YY, Jia YZ, et al. Effect of Coal-Rock Interface on Hydralnic Fracturing Propagation. Journal of Northeastern UniVersity (Natural Science). 2014,35:1340-1345.

[47] Madenci E, Oterkus E. Peridynamic Theory and Its Applications. New York: Springer, 2014.

[48] Silling SA. Reformulation of elasticity theory for discontinuities and long-range forces. Journal of Mechanics Physics of Solids. 2000,48:175-209.

[49] Silling SA, Lehoucq RB. Peridynamic Theory of Solid Mechanics. Advances in Applied Mechanics. 2010,44:73-168.

[50] Qin M, Yang D, Chen W. Three-dimensional hydraulic fracturing modeling based on peridynamics. Engineering Analysis with Boundary Elements. 2022,141:153-166.

[51] Qin M, Yang D, Chen W, et al. Hydraulic fracturing network modeling based on peridynamics. Engineering Fracture Mechanics. 2021,247.

[52] Qin M, Yang D. Numerical investigation of hydraulic fracture height growth in layered rock based on peridynamics. Theoretical and Applied Fracture Mechanics. 2023,123.

[53] Qin M, Yang D, Chen W. Numerical investigation of the effects of fracturing fluid parameters on hydraulic fracture propagation in jointed rock mass based on peridynamics. Engineering Analysis with Boundary Elements. 2022,135:38-51.

[54] Madenci E, Oterkus E. Peridynamic theory and its applications. New York: Springer Scienc, 2014.

[55] Qin MQ, Yang DS, Chen WZ, et al. Hydraulic fracturing model of a layered rock mass based on peridynamics. Engineering Fracture Mechanics. 2021,258.

[56] Qin MQ, Yang DS, Chen WZ. Three-dimensional hydraulic fracturing modeling based on peridynamics. Engineering Analysis with Boundary Elements. 2022,141:153-166.

[57] Qin M, Yang D. Numerical investigation of hydraulic fracture height growth in layered rock based on peridynamics. Theoretical and Applied Fracture Mechanics. 2023,125:103885.

[58] Qin M, Yang D. Numerical investigation of hydraulic fracturing in a heterogeneous rock mass based on peridynamics. Rock Mechanics and Rock engineering. 2023,56:4485-4505.

[59] Bobaru F, Foster JT, Geubelle PH, et al. Handbook of peridynamic modeling.

Boca Raton: Crc Press, 2016.

[60] Kilic B, Madenci E. An adaptive dynamic relaxation method for quasi-static simulations using the peridynamic theory. Theoretical and Applied Fracture Mechanics. 2010,53:194-204.

[61] Qin M, Yang D, Yang S. Hydraulic fracturing model of a layered rock mass based on peridynamic. Engineering Fracture Mechanics. 2021,258.

[62] Qin MQ, Yang DS, Chen WZ, et al. Hydraulic fracturing network modeling based on peridynamics. Engineering Fracture Mechanics. 2021,247.

[63] Gerstle W, Sau N, Aguilera E. Micropolar peridynamic constitutive model for concrete. Transactions, SMiRT 19. Toronto2007.

[64] Renshaw CE, Pollard DD. An experimentally verified criterion for propagation across unbounded frictional interfaces in brittle, linear elastic materials. International Journal of Rock Mechanics & Mining ence & Geomechanics Abstracts. 1995,32:237-249.

[65] Hu J, Garagash DI. Plane-strain propagation of a fluid-driven crack in a permeable rock with fracture toughness. Journal of Engineering Mechanics. 2010,136:1152-1166.

[66] Sundaram BM, Tippur HV. Dynamic crack propagation in layered transparent materials studied using digital gradient sensing method. Proceedings of the 2014 Annual Conference on Experimental and Applied Mechanics: Springer International Publishing, 2015. p. 197-205.

[67] Smith MB, Montgomery CT. Hydraulic fracturing. New York: CRC Press, 2015.

[68] Zhou Y, Yang D, Zhang X, et al. Numerical investigation of the interaction between hydraulic fractures and natural fractures in porous media based on an enriched FEM. Engineering Fracture Mechanics. 2020,235.

[69] Zhang F, Damjanac B, Maxwell S. Investigating hydraulic fracturing complexity in naturally fractured rock masses using fully coupled multiscale numerical modeling. Rock Mechanics and Rock Engineering. 2019,52:5137–5160.

[70] Khoei AR, Vahab M, Hirmand M. Modeling the interaction between fluid-driven fracture and natural fault using an enriched-FEM technique. International Journal of Fracture. 2015,197:1-24.

[71] Beugelsdijk LJL, De Pater CJ, Sato K. Experimental hydraulic fracture propagation in a multi-fractured medium. SPE Asia Pacific conference on integrated modelling for asset managemen: SPE, 2000.

[72] Fan T, Zhang G. Influence of injection rate and fracturing fluid viscosity on hydraulic fracture geometry in coal. Journal of China University of Petroleum. 2014,38:117-123.

Highlights

(1) A self-developed peridynamics-based 2D/3D hydraulic fracturing model to simulate fracture propagation in fractured rock.

(2) The hydro-mechanical coupling mechanism of the interaction between hydraulic fracture and natural fracture is revealed.

(3) The interaction modes between fractures in a 3D rock mass are explored, including scenarios where the hydraulic fracture bypasses the natural fracture.

(4) The propagation of intricate fracture networks in a 3D fractured rock mass is simulated.